

DTIC FILE COPY

4

SEVERN COMMUNICATIONS
CORPORATION

Astronaut Radiation Exposure in Low-Earth Orbit

Part I: Galactic Cosmic Radiation

AD-A204 598

SCC Report 88-01

31 March 1988

DTIC
ELECTE
1 FEB 1989
S D
E

SEVERN COMMUNICATIONS CORPORATION

223 Benfield Park Drive
Millersville, Maryland 21108

89 2 1 075

Report Documentation Page

Report: SCC 88-01

Date: 31 March 1988

Title: Astronaut Radiation Exposure in Low-Earth Orbit,
Part I: Galactic Cosmic Radiation

Author: John R. Letaw
Severn Communications Corporation
223 Benfield Park Drive
Millersville, MD 21108

Contract: #N00014-87-C-2251
Naval Research Laboratory
4555 Overlook Avenue, S.W.
Washington, DC 20375

Abstract: *Cont'd from pg. 3* Linear energy transfer (LET) spectra, absorbed dose, and dose equivalent from galactic cosmic radiation and its fragments are presented for four, representative low earth orbit configurations. The orbits include a high (STS-51J) and low (STS-61C) altitude, low-inclination (28.5°) flight; a high-inclination (49.5°) flight (STS-51F); and a polar flight. Results are compared with computations for an exo-magnetospheric flight. *(deg)*

ASTRONAUT RADIATION EXPOSURE

IN LOW-EARTH ORBIT

PART I: GALACTIC COSMIC RADIATION

SCC Report 88-01

31 March 1988

Accession For	
NTIS GRA&I	<input checked="" type="checkbox"/>
DTIC TAB	<input type="checkbox"/>
Unannounced	<input type="checkbox"/>
Justification	<input checked="" type="checkbox"/>
By _____	
Distribution/	
Availability Codes	
Dist	Avail and/or Special
A-1	

Severn Communications Corporation
223 Benfield Park Drive
Millersville, Maryland 21108



TABLE OF CONTENTS

INTRODUCTION	3
METHOD OF CALCULATION	5
LET SPECTRA	16
ABSORBED DOSE AND DOSE EQUIVALENT	28
SUMMARY AND CONCLUSIONS	42
REFERENCES	43

INTRODUCTION

In recent years, there has been increasing concern about the radiation doses which will be suffered by astronauts on present-day and future space missions (e.g., Letaw, Silberberg and Tsao, 1987). Future space operations will differ in many respects from previous programs:

- On the Space Station, crew stays of up to one year greatly exceed the length of previous missions. Consequently, the total absorbed dose for these missions is expected to increase proportionately.
- Manned missions into unfamiliar space environments are now being contemplated. These missions include polar orbits, geosynchronous orbit, lunar bases, and a manned Mars mission. Radiation in these environments is qualitatively different from that encountered in low-altitude, low-inclination orbits.
- As our commitment to space exploration increases, the space population will increase thereby magnifying the consequences of any radiation exposure. Furthermore, many space travelers will be classified as civilian space workers, rather than astronaut-explorers, and will be subject to more rigorous radiation dose limits.
- The effect of the heavy-ion component of space radiation on human health is not well understood. This component is rarely encountered by terrestrial workers, hence epidemiological data are unavailable. Tissue experiments suggest that present radiation protection practice (quality factor and dose equivalent) may be inadequate for characterizing the health risks of heavy ion exposures.

In the wake of this new awareness of risks, there has been increased activity in the study of space radiation and its biological effects. The US National Commission on Radiation Protection and Measurement (NCRP) has undertaken to assess the risks of space radiation to astronauts (Fry, 1986). They have recommended an annual dose limit of 50 rem (to the blood-forming organs, or red bone marrow) from all sources for astronauts on future missions. Also recommended are annual limits for the eye lens and skin, as well as monthly and career limits. New efforts to compile space radiation exposure data and to assemble interested scientists in many associated fields have been initiated (McCormack, Swenberg and Bucker, 1988). Space radiation has been recognized as a fundamental concern by NASA early in manned Mars mission planning (Letaw, Silberberg and Tsao, 1986).

In order to characterize radiation exposure risks on space missions one requires models of space radiation environments, codes for transporting the components of ionizing radiation, and procedures for assessing radiation risks of a given exposure. To verify their accuracy, predictions based on these transport results must then be compared with existing dosimetry data,

This is the first in a series of reports in which LET spectra for several missions in low-Earth orbit are computed and compared with measured dosimetry data. The missions chosen for this comparison are the shuttle flights (a) STS-51F, high-inclination (49.5°), low-altitude (~ 320 km) orbit, (b) STS-51J, low-inclination (28.5°), high-altitude (~ 500 km) orbit, (c) STS-61C, low-inclination (28.5°), low-altitude (~ 320 km) orbit, and (d) a hypothetical polar orbit (90° inclination). These missions are expected to exhibit a range of relative contributions of galactic cosmic radiation and trapped proton exposure. Previous comparisons of exo-magnetospheric flight data have been presented by Letaw and Adams (1986 a,b).

In this report, the contribution of galactic cosmic radiation and its spallation fragments to radiation doses and LET spectra are computed. The other major components, trapped protons and secondary particles emitted from the shielding material, will be considered in later reports. Galactic cosmic radiation dominates the dose equivalent on a manned Mars mission and in polar orbit; trapped protons become increasingly important in higher altitude and lower inclination orbits. Target secondaries - protons, neutrons, pions, and recoil nuclei - result from nuclear collisions of either trapped protons or galactic cosmic radiation in the dosimeter and shielding material.

METHOD OF CALCULATION

Methods used to calculate the galactic cosmic radiation (GCR) dose to astronauts have been described in several previous reports (Letaw, Silberberg and Tsao, 1988; Letaw and Clearwater, 1986; Silberberg et al., 1984). The three-part process includes specifying the radiation environment, transporting the radiation components through shielding, and computing energy-deposition rates (LET spectra and radiation dose) in a tissue-like material.

The galactic cosmic radiation environment model (CREME) used in this study has been developed by the Naval Research Laboratory (Adams, Silberberg and Tsao, 1981). Radiation fluxes at solar minimum have been used throughout. Galactic cosmic radiation is at its maximum intensity during the solar minimum. Therefore, use of the solar minimum flux represents nearly an upper limit on galactic cosmic radiation exposure. The specific missions under study occurred between July, 1985 and January, 1986, very near the predicted solar minimum of the model.

The precise GCR exposure on a space mission is determined by the spacecraft orbital parameters. The "geomagnetic cutoff" limits the transmission of lower-energy cosmic radiation into the magnetosphere and modifies the GCR spectrum. Another modifying factor is the Earth's shadow which prevents GCR from reaching a low-Earth orbiting craft from approximately 40% of the solid angle. These factors have been discussed by Adams, Letaw and Smart (1983) and Letaw et al. (1985). Orbital parameters used in this study are shown in Table 1.

The computer code, UPROP, used to perform transport computations in this report provides an exact, numerical solution of the equation:

$$\frac{\partial J_i}{\partial x} = -r_i J_i + \sum_j r_{ij} J_j + \frac{\partial}{\partial E} [s_i J_i]$$

where J_i are the cosmic-ray fluxes with subscript i equal to the charge ($1 \leq i \leq 28$). The independent variable x is the pathlength in the transport medium and is usually expressed in units of $g \text{ cm}^{-2}$. r_i is the rate of loss of species i due to nuclear fragmentation, and is proportional to the total charge-changing cross section in the transport medium. r_{ij} is the rate of gain of species i due to nuclear fragmentation of other species j , and is proportional to the partial cross sections. s_i is the stopping power, or energy loss rate, of species i in the transport medium. All quantities in this equation are energy dependent. The solution is obtained over energies per nucleon in the range $1 \text{ MeV} \leq E \leq 100 \text{ GeV}$.

The transport medium chosen for this report is aluminum, a major structural material in most spacecraft. Energy loss rates are taken from equations presented in Ahlen (1980) and Ziegler (1980). They are in excellent agreement with the tables of Northcliffe and Schilling (1970). Figure 1 shows the stopping powers in aluminum for several important cosmic-ray ion species.

TABLE 1

ADOPTED ORBITAL PARAMETERS

<u>Flight</u>	<u>Date</u>	<u>Inclination</u>	<u>Altitude</u>	<u>Duration</u>
STS-61C	12JAN86	28.5°	324 km	146 hr
STS-51J	03OCT85	28.5°	510 km	95 hr
STS-51F	29JUL85	49.5°	322 × 304 km	191 hr
POLAR	solar min.	90.0°	300 km	-
EXO- MAGNETOSPHERE	solar min.	-	(outside magnetosphere)	-

The partial fragmentation cross sections used in this report are based on the Silberberg and Tsao (1973) semi-empirical formulas (see also Silberberg, Tsao and Letaw, 1985) which have been modified for nucleus-nucleus collisions (Silberberg and Tsao, 1977). Examples of these cross sections for different projectiles are shown in Figure 2 (carbon on aluminum), Figure 3 (oxygen on aluminum), Figure 4 (iron on aluminum), and Figure 5 (iron on sulfur). The latter is included because experimental data are available for comparison. The model agrees reasonably well with data (Olson et al., 1983; Westfall et al., 1979) over a wide range of product charges.

Cross sections for the production of light nuclides ($1 \leq Z \leq 2$) are obtained in the process of normalizing the total inelastic cross section to partial fragmentation cross sections according to the method of Letaw (1983). The charge-changing cross sections are obtained from Westfall's et al. (1979) mass-changing cross section modified by subtraction of charge-preserving cross sections obtained from the Silberberg and Tsao formulas. The energy-dependent total inelastic cross section for protons on aluminum is obtained from Letaw, Silberberg, and Tsao (1983). Figure 6 shows the total inelastic cross sections on aluminum as adopted for this report.

In the terminology of this report "primary cosmic radiation" refers to GCR particles which have not undergone charge-changing nuclear reactions in shielding. "Fragments" are pieces of cosmic-ray heavy ions that have broken up in nuclear reactions in the shielding. Fragments continue to be transported through the shielding with the velocity of their progenitors and may fragment again. Fragments are one type of GCR secondary. Target secondaries consist of

protons, neutrons, pions, and heavy ion recoils which were originally part of the shielding and have been accelerated by nuclear reactions with cosmic radiation. Target secondaries will be treated in detail in a later report.

In this report, GCR fluxes are transported through 19 thicknesses of aluminum: 0, 1, 2, 3, 4, 5, 10, 15, 20, 25, 30, 35, 40, 45, 50, 60, 70, 80, and 90 g cm⁻². The resulting fluxes have been converted into several quantities of interest in radiation protection studies: LET spectra, absorbed dose, and dose equivalent. The LET spectrum represents fluxes according to the rate at which particles deposit energy in some material (water is used in this report). Heinrich (1988 and references therein) has described the use and importance of the GCR LET spectrum. Conversion of fluxes to LET spectra in water is accomplished using the stopping power of heavy ions in water. These stopping powers are obtained as described above and are shown in Figure 7.

The absorbed dose is an integral measure of energy deposited per unit mass of material. SI units for absorbed dose are 1 Gray = 1 joule kg⁻¹ (1 cGy = 1 rad). For radiation protection purposes (ICRP, 1977), an LET-dependent quality factor is defined to more closely correlate the dose with long-term biological effects. The quality factor is a number between 1 and 20 which multiplies the absorbed dose. The resulting quantity is the dose equivalent. SI units for dose equivalent are 1 Sievert = 1 joule kg⁻¹ (1 cSv = 1 rem). The quality factor provides only a rough measure of the relative biological effectiveness (RBE) of heavy ion species and should not be confused with RBE, which is a function of many experimental factors. The dose equivalent is designed exclusively for radiation protection applications. Figure 8 shows the quality factor adopted by the ICRP (1977) and another quality factor proposed in a report by the International Commission on Radiation Units and Measurements (ICRU, 1986).

The ICRU quality factor (ICRU-QF) differs from the ICRP quality factor (ICRP-QF) in several ways. Around 100 keV μm⁻¹ (about the stopping power of relativistic iron) the ICRU-QF peaks at 25, about 20% greater than the maximum ICRP-QF. In this important range, the ICRU-QF is about twice as large as the ICRP-QF. The ICRU-QF decreases above this range reducing the risk associated with slow and stopping heavy ions. The ICRU-QF for relativistic protons (0.2 keV μm⁻¹) is about 0.05, a factor of 20 below the standard X-rays or γ-rays. Radiation dose equivalents computed using the ICRU-QF are significantly larger than when using the standard ICRP-QF. We recommend great care in the adoption of new quality factors for use in GCR risk estimation, since minor changes may have far-reaching consequences. The ICRP-QF is used exclusively in this report.

FIGURE 1
STOPPING POWER IN ALUMINUM

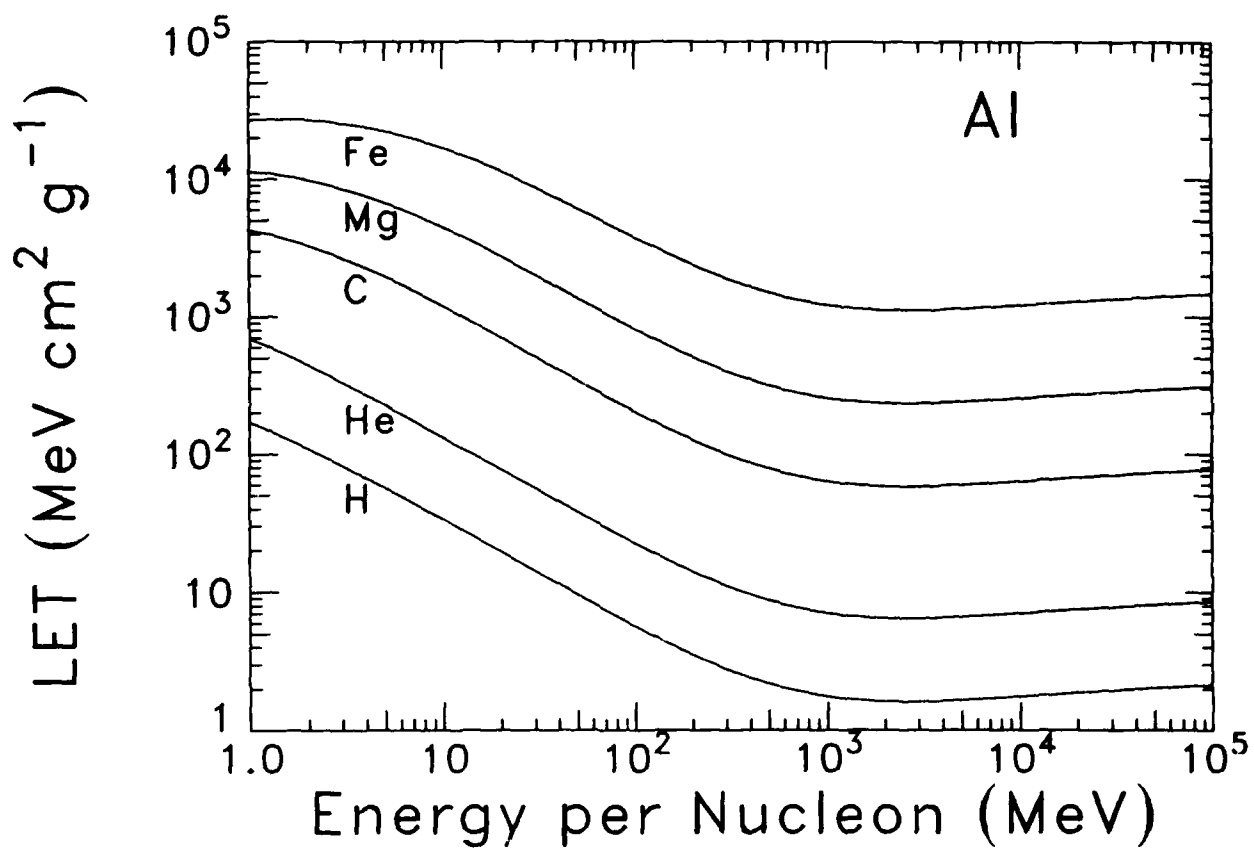


FIGURE 2
PARTIAL CROSS SECTIONS FOR CHARGED-FRAGMENT PRODUCTION IN
NUCLEAR COLLISIONS OF CARBON ON ALUMINUM

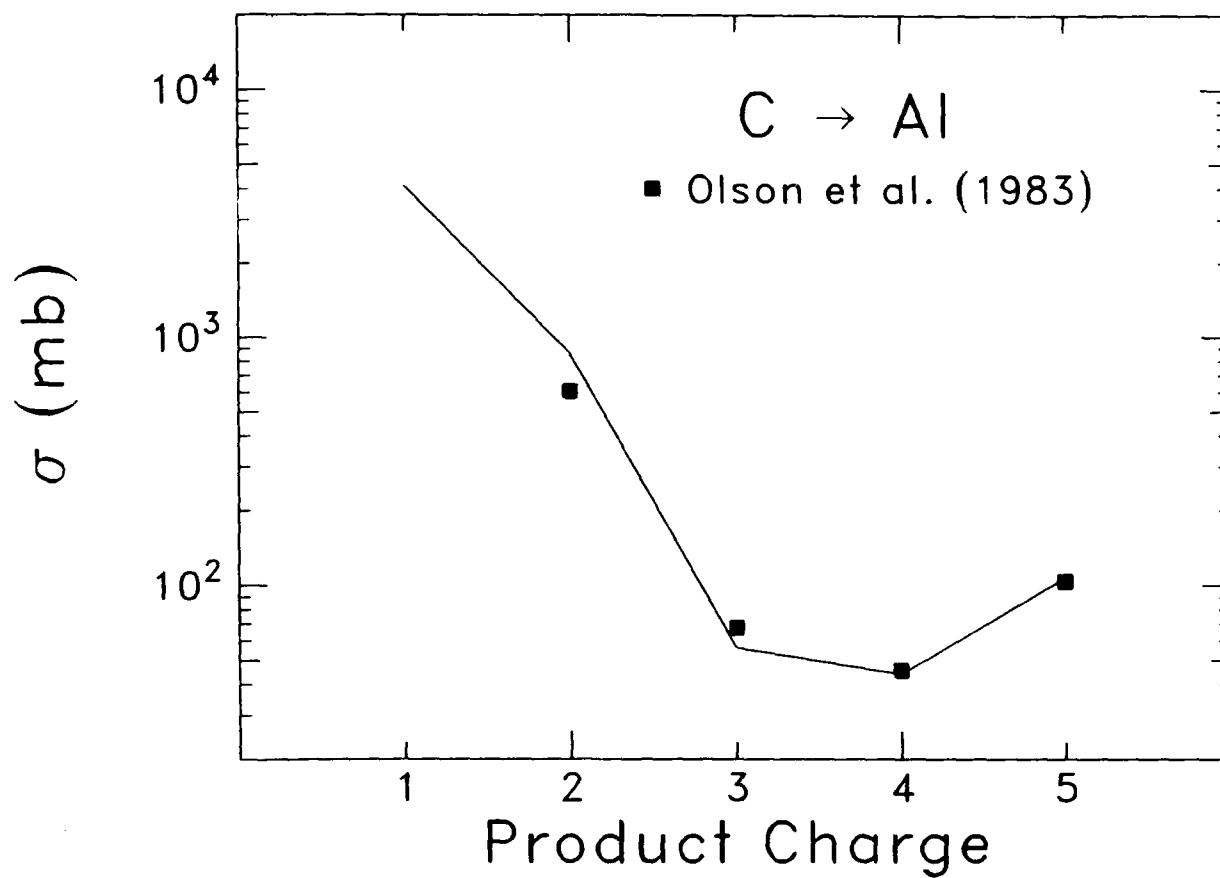


FIGURE 3
PARTIAL CROSS SECTIONS FOR CHARGED-FRAGMENT PRODUCTION IN
NUCLEAR COLLISIONS OF OXYGEN ON ALUMINUM

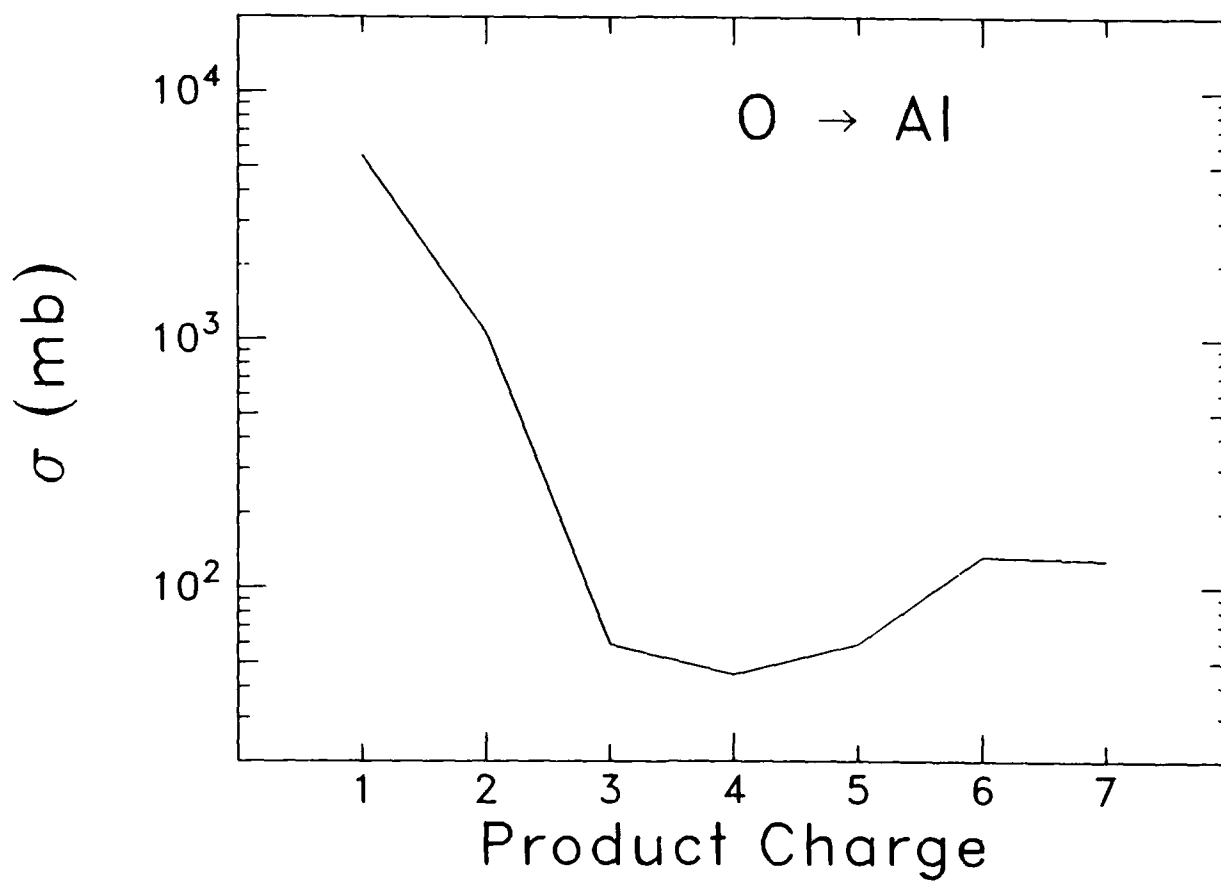


FIGURE 4
PARTIAL CROSS SECTIONS FOR CHARGED-FRAGMENT PRODUCTION IN
NUCLEAR COLLISIONS OF IRON ON ALUMINUM

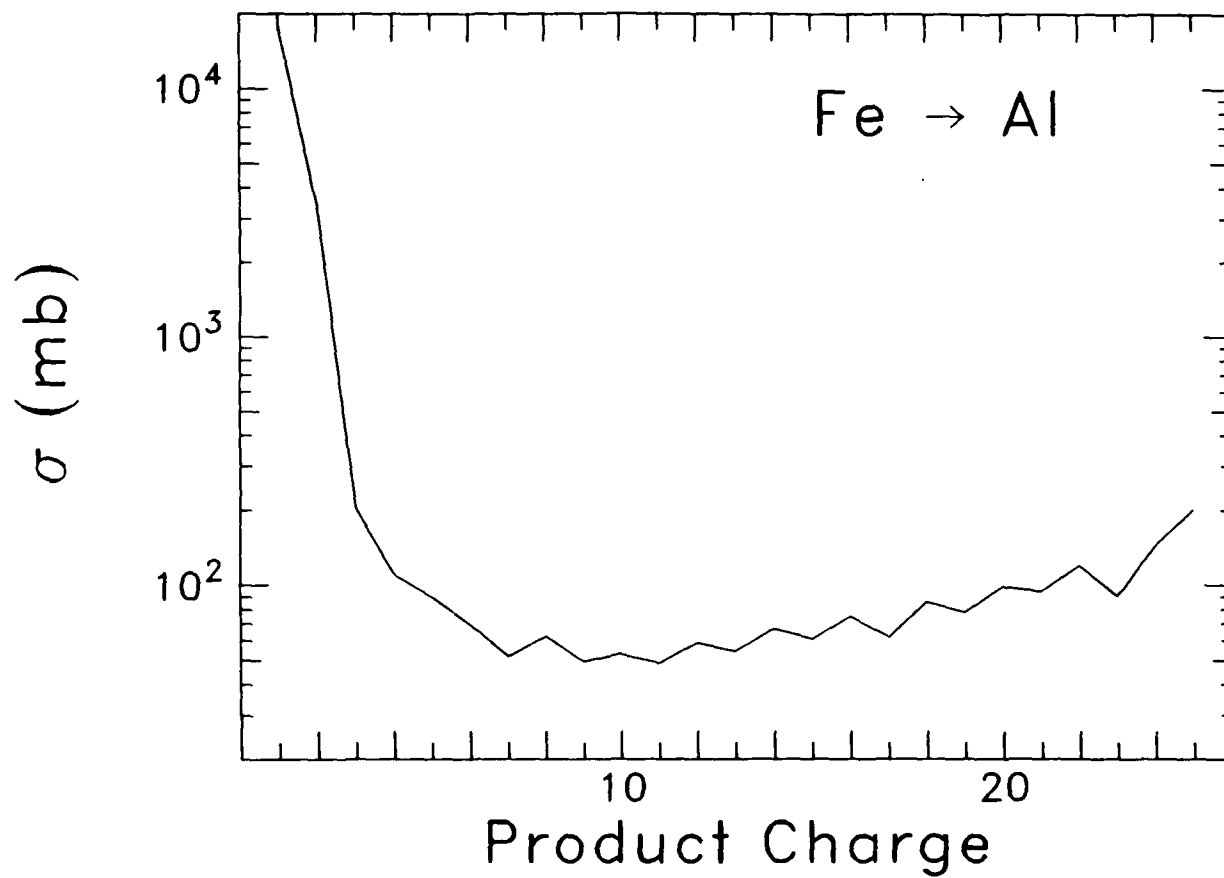


FIGURE 5
PARTIAL CROSS SECTIONS FOR CHARGED-FRAGMENT PRODUCTION IN
NUCLEAR COLLISIONS OF IRON ON SULFUR

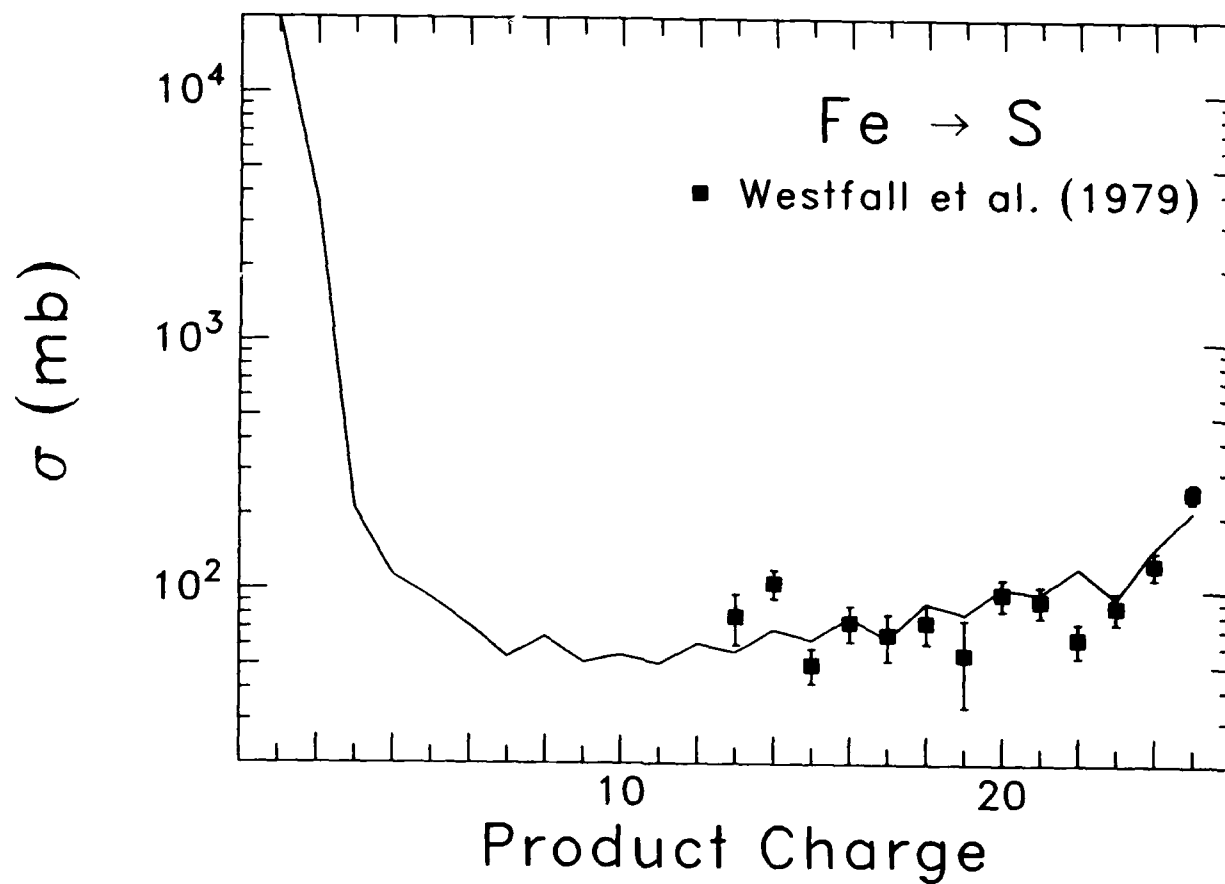


FIGURE 6
TOTAL INELASTIC CROSS SECTION FOR FRAGMENTATION OF
HEAVY IONS ON ALUMINUM

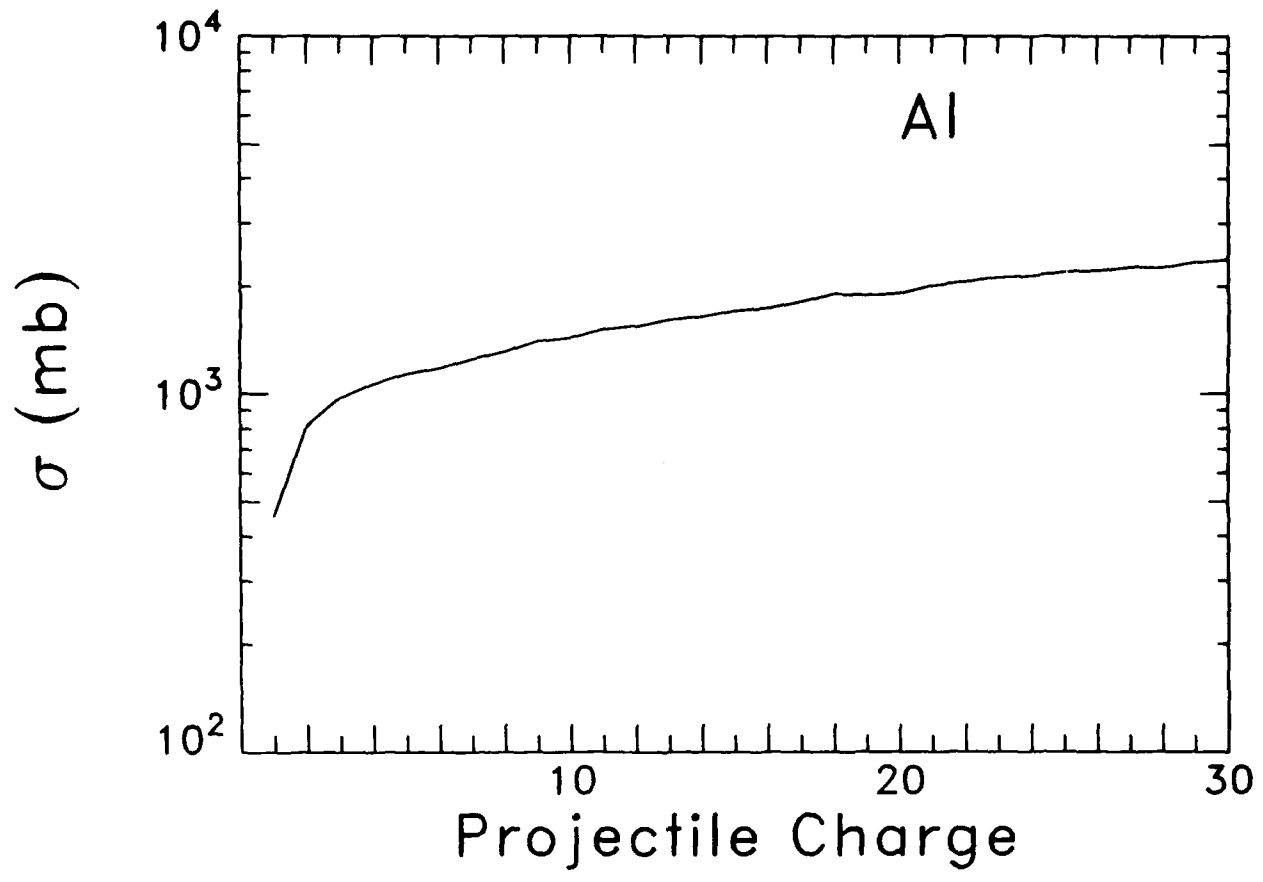


FIGURE 7
STOPPING POWER IN WATER

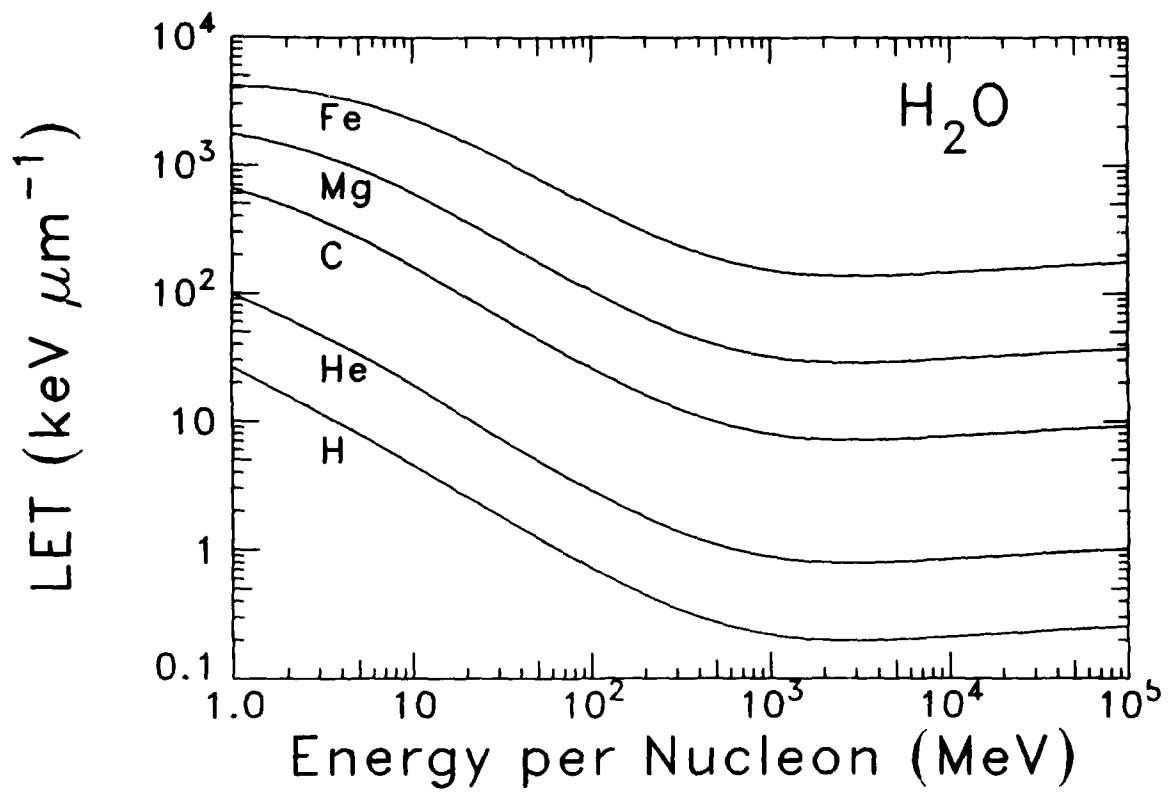
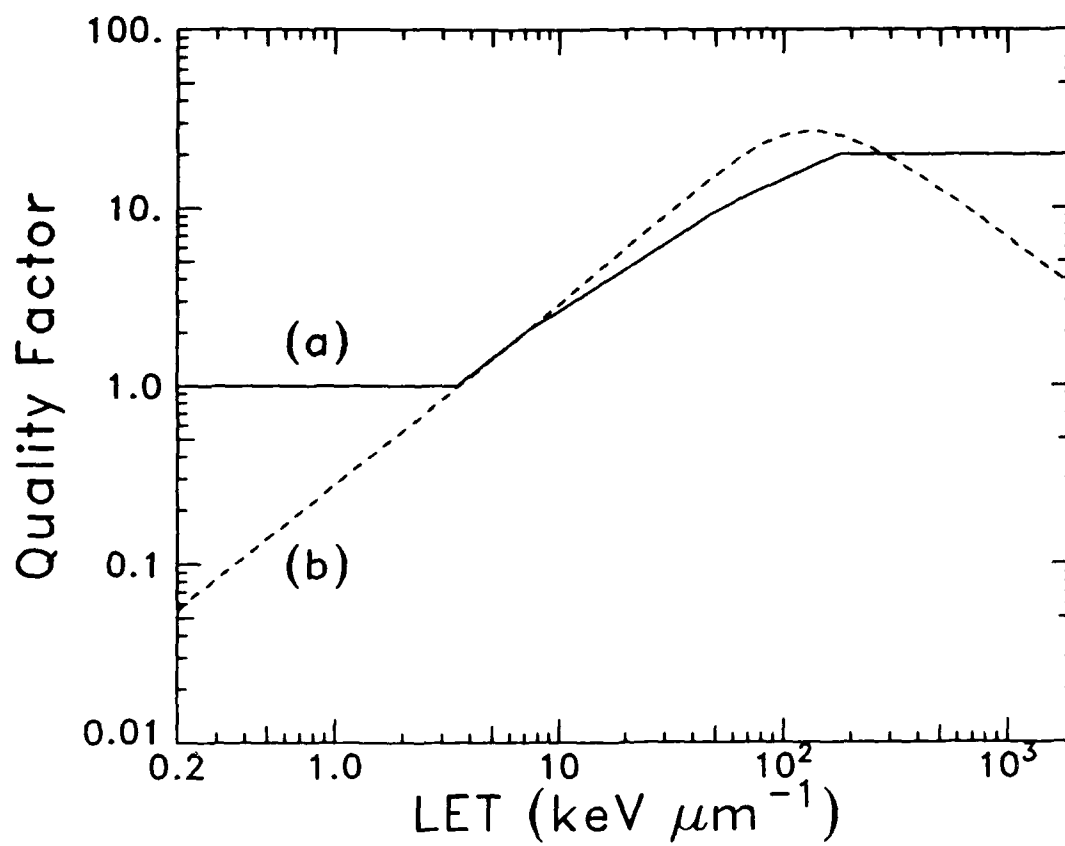


FIGURE 8
QUALITY FACTORS FOR USE IN RADIATION PROTECTION



LET SPECTRA

Linear energy transfer (LET) spectra of GCR in water for the orbits examined in this report are shown in Figures 9 through 18. The figures show LET spectra for GCR primaries (particles which have undergone no nuclear interactions), GCR fragments (secondary and higher order cosmic-ray fragmentation products), and the sum of these two spectra. The primary and sum spectra descend in 10 g cm^{-2} increments from 0 g cm^{-2} through 90 g cm^{-2} . The fragment spectra vary in a complex manner with pathlength and are shown at 10, 50, and 90 g cm^{-2} . No fragments occur in the 0 g cm^{-2} spectrum.

Figure 9 (STS-61C) exhibits the typical step-like structure of an LET spectrum in low-inclination orbit. An abrupt step occurs at about $2 \text{ MeV cm}^2 \text{ g}^{-1}$ where relativistic protons are incorporated into the integral spectrum. Another step occurs at about $8 \text{ MeV cm}^2 \text{ g}^{-1}$ where relativistic helium ions add to the spectrum. Steps are more or less pronounced according to the abundance of a cosmic-ray species relative to that of higher charge species. The step at about $1300 \text{ MeV cm}^2 \text{ g}^{-1}$ is due to relativistic iron. A high-LET tail in the spectrum begins to appear after about 50 g cm^{-2} because near-relativistic ions have slowed and therefore lose energy at a greater rate.

Figure 10 (STS-61C) shows the decomposition of the LET spectrum into primary GCR and GCR fragments. The spectra are similar in appearance. Fragments make a small contribution to the LET spectrum. The high-LET fragments exist nearly in equilibrium between 10 and 50 g cm^{-2} . The proton fragments exist nearly in equilibrium between 50 and 90 g cm^{-2} . The equilibrium is determined by the competition between production through nuclear fragmentation and ionization loss.

Figures 11 and 12 (STS-51J) are similar to Figures 9 and 10 (STS-61C), respectively, because these shuttle flights differed only in altitude. Particle fluxes are slightly higher on the $\sim 500 \text{ km}$ flight of STS-51J because the solid angle obstructed by the Earth is slightly smaller.

The LET spectra of STS-51F (Figures 13 and 14) show much more gradual steps than those of the lower inclination orbits. The high-LET regions containing no particles in the 0 g cm^{-2} spectrum are rapidly filled in the other spectra due to slowing down of heavy ions in the shielding. Shielding may therefore increase the probability of threshold radiation effects at orbital inclinations near 50° .

LET spectra for a polar orbit are shown in Figures 15 and 16. The 0 g cm^{-2} spectrum is somewhat unphysical at higher LETs because it was not possible to characterize the low-energy per nucleon ($1 \text{ MeV} \leq E \leq 10 \text{ MeV}$) fluxes of cosmic radiation. In the CREME model, the flux is taken to be constant below 10 MeV per nucleon. Particles with $E \leq 10 \text{ MeV}$ are rapidly stopped in shielding, thus

for greater shielding depths the spectra are accurate. It is noteworthy that the polar LET spectra are attenuated faster than low-inclination spectra because of the large contribution of low-energy, high-LET particles.

The exo-magnetospheric LET spectra are shown for comparison in Figures 17 and 18. These spectra are not attenuated by the Earth's magnetic field and the Earth's shadow. The 0 g cm^{-2} spectrum is somewhat unphysical for the same reasons as the polar LET spectrum. The exo-magnetospheric LET spectra are applicable to missions outside the magnetosphere, such as a manned Mars or Moon mission, and missions to geosynchronous orbit. On the surface of other planets, atmospheric attenuation and planetary shadowing must be taken into account. The exo-magnetospheric spectra are essentially upper limits of GCR exposure.

The total GCR particle fluxes in the LET spectra above are ordered exo-magnetospheric > polar > STS-51F (49.5°) > STS-51J (28.5°, ~ 500 km) > STS-61C (28.5°, ~ 300 km). This ordering is directly correlated with the deflection of particles from the Earth's magnetic field and the shadow effect of the body of the Earth. Including the different shielding thicknesses, the LET spectra vary by two orders of magnitude in intensity. They have qualitatively different shapes depending on the presence or absence of low-energy (high-LET) ions.

FIGURE 9
LET SPECTRA OF GALACTIC COSMIC RADIATION
STS-61C

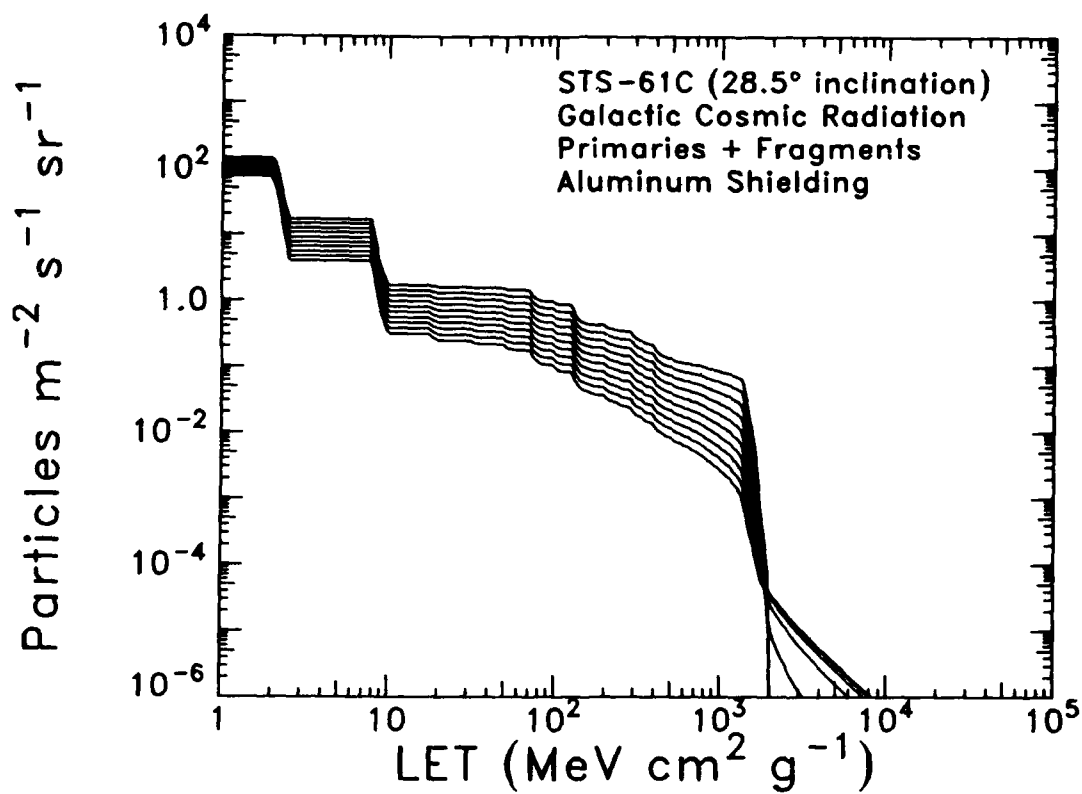


FIGURE 10
 LET SPECTRA OF GALACTIC COSMIC RADIATION
 DECOMPOSITION INTO PRIMARIES AND FRAGMENTS

STS-61C

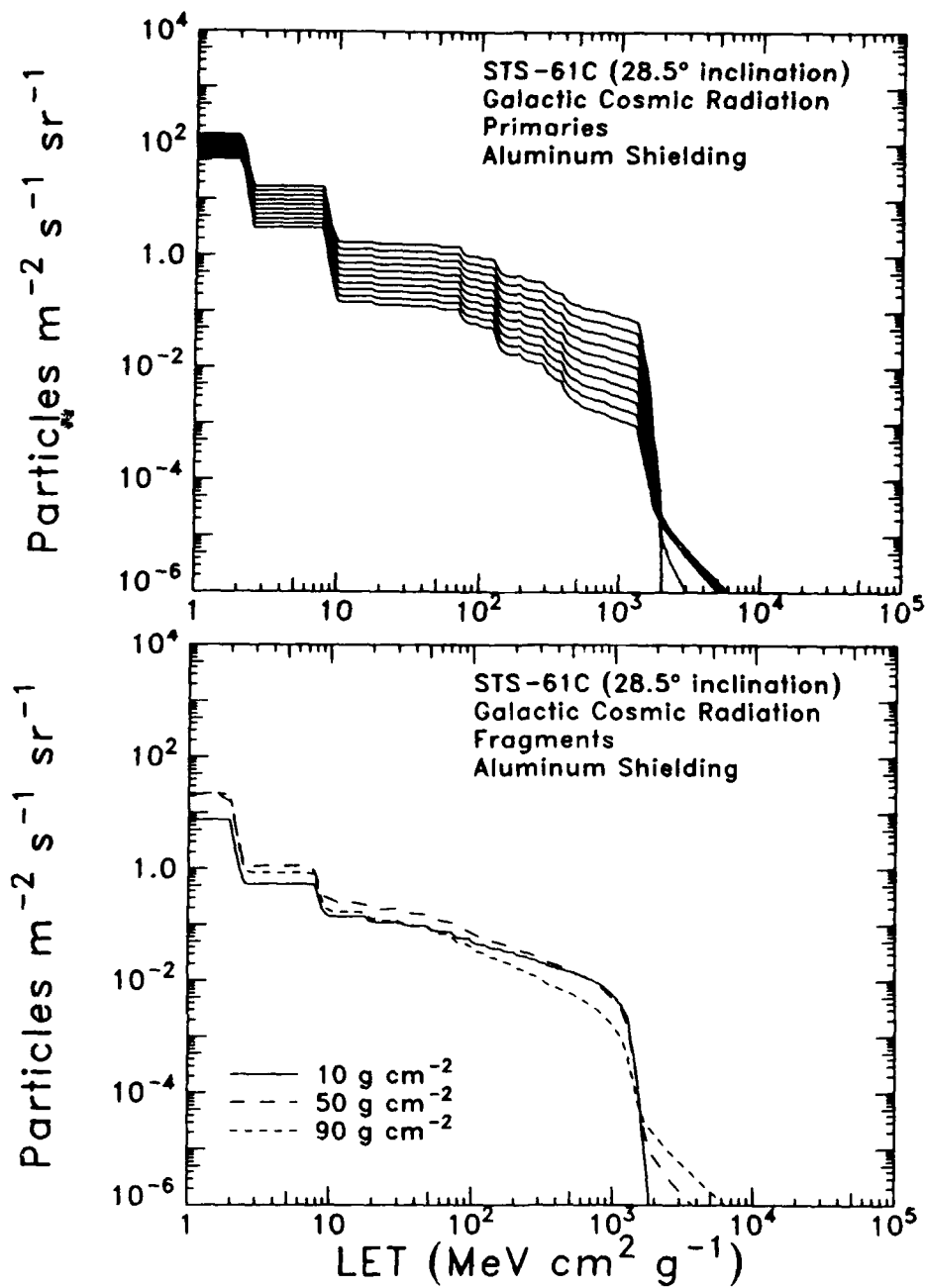


FIGURE 11
LET SPECTRA OF GALACTIC COSMIC RADIATION
STS-51J

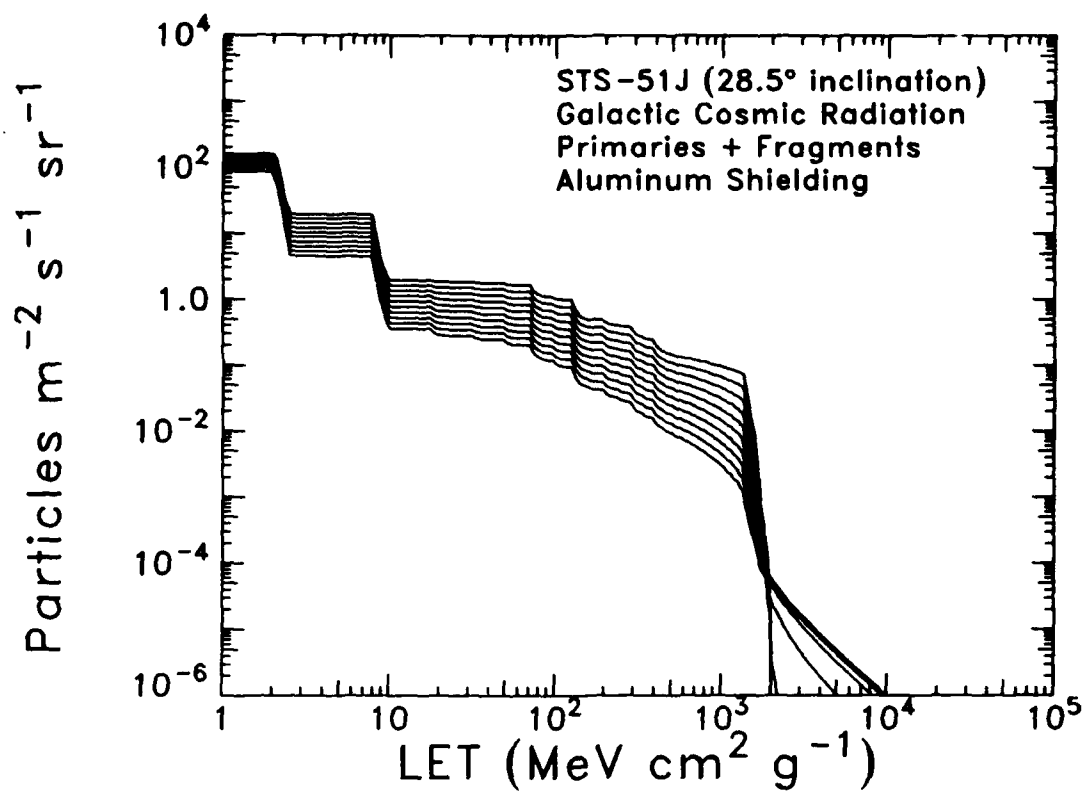


FIGURE 12

LET SPECTRA OF GALACTIC COSMIC RADIATION
DECOMPOSITION INTO PRIMARIES AND FRAGMENTS

STS-51J

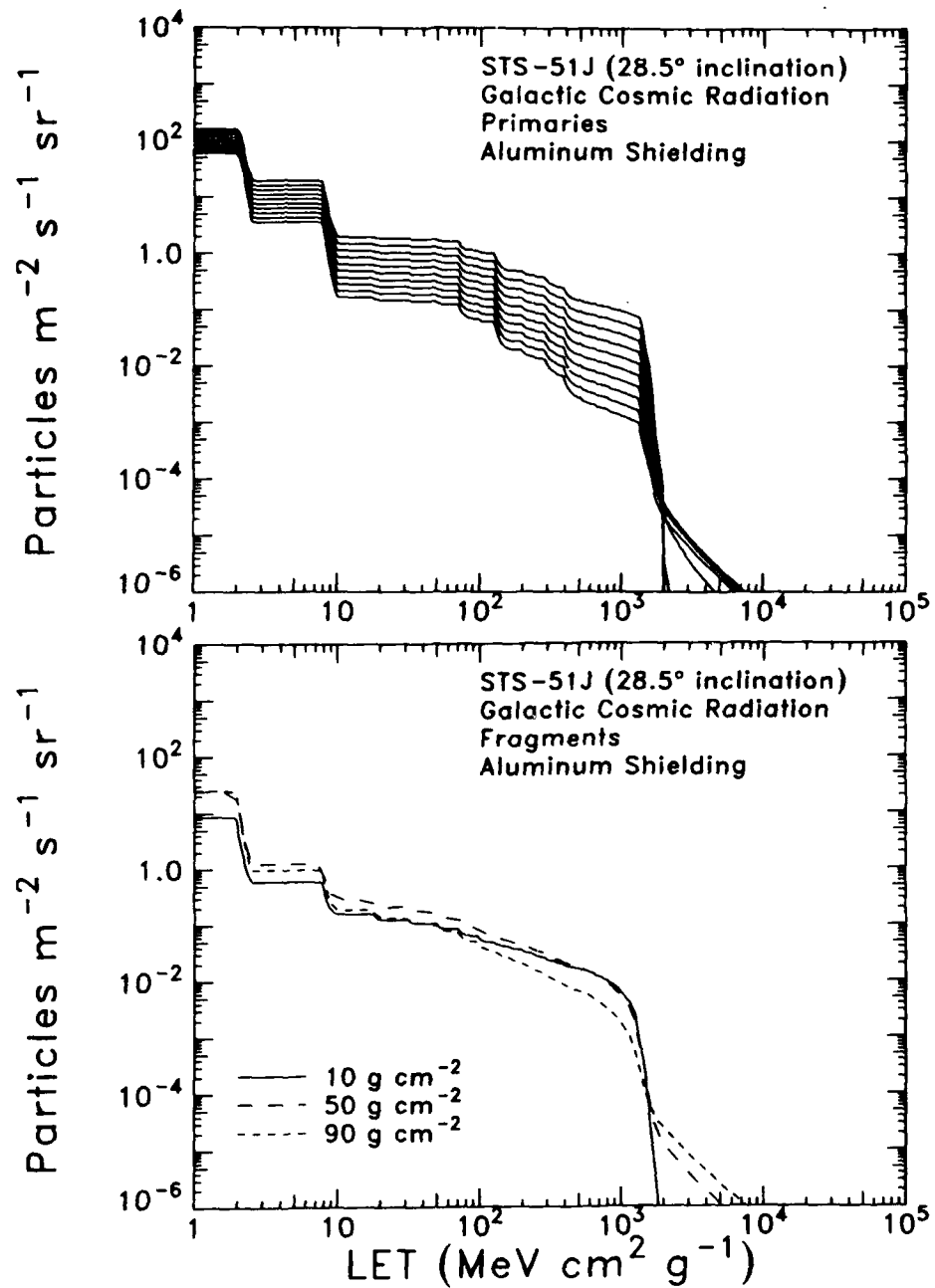


FIGURE 13
LET SPECTRA OF GALACTIC COSMIC RADIATION
STS-51F

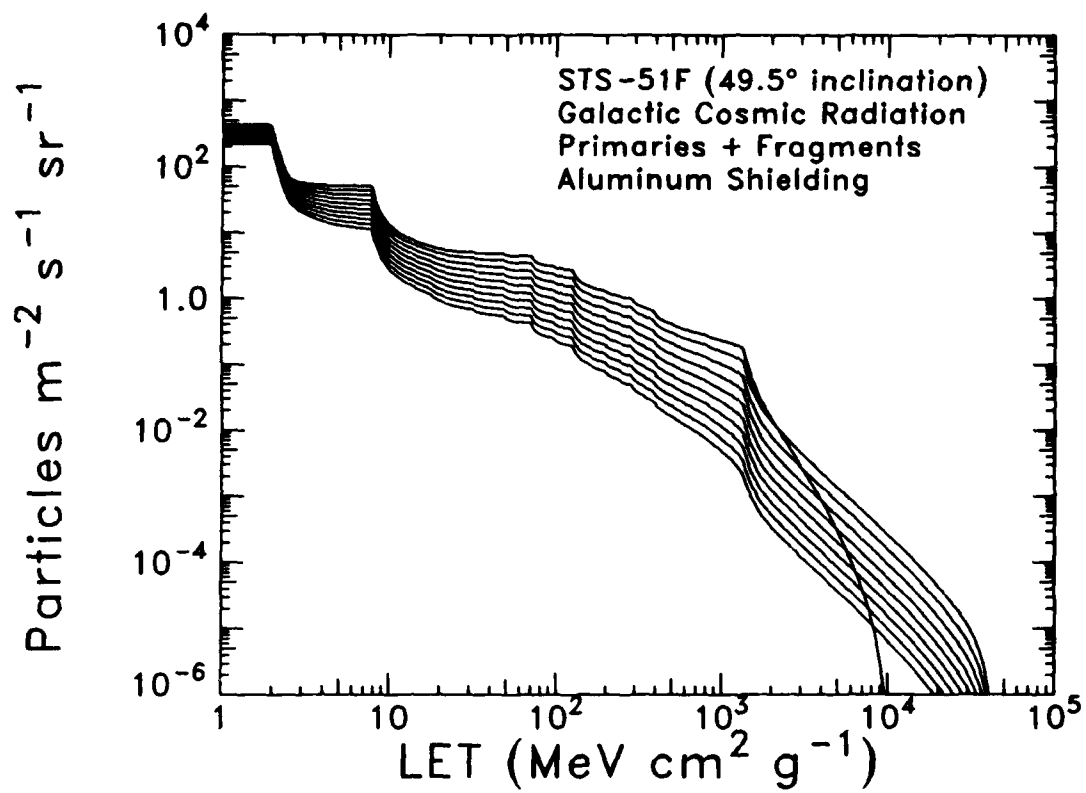


FIGURE 14

LET SPECTRA OF GALACTIC COSMIC RADIATION
DECOMPOSITION INTO PRIMARIES AND FRAGMENTS

STS-51F

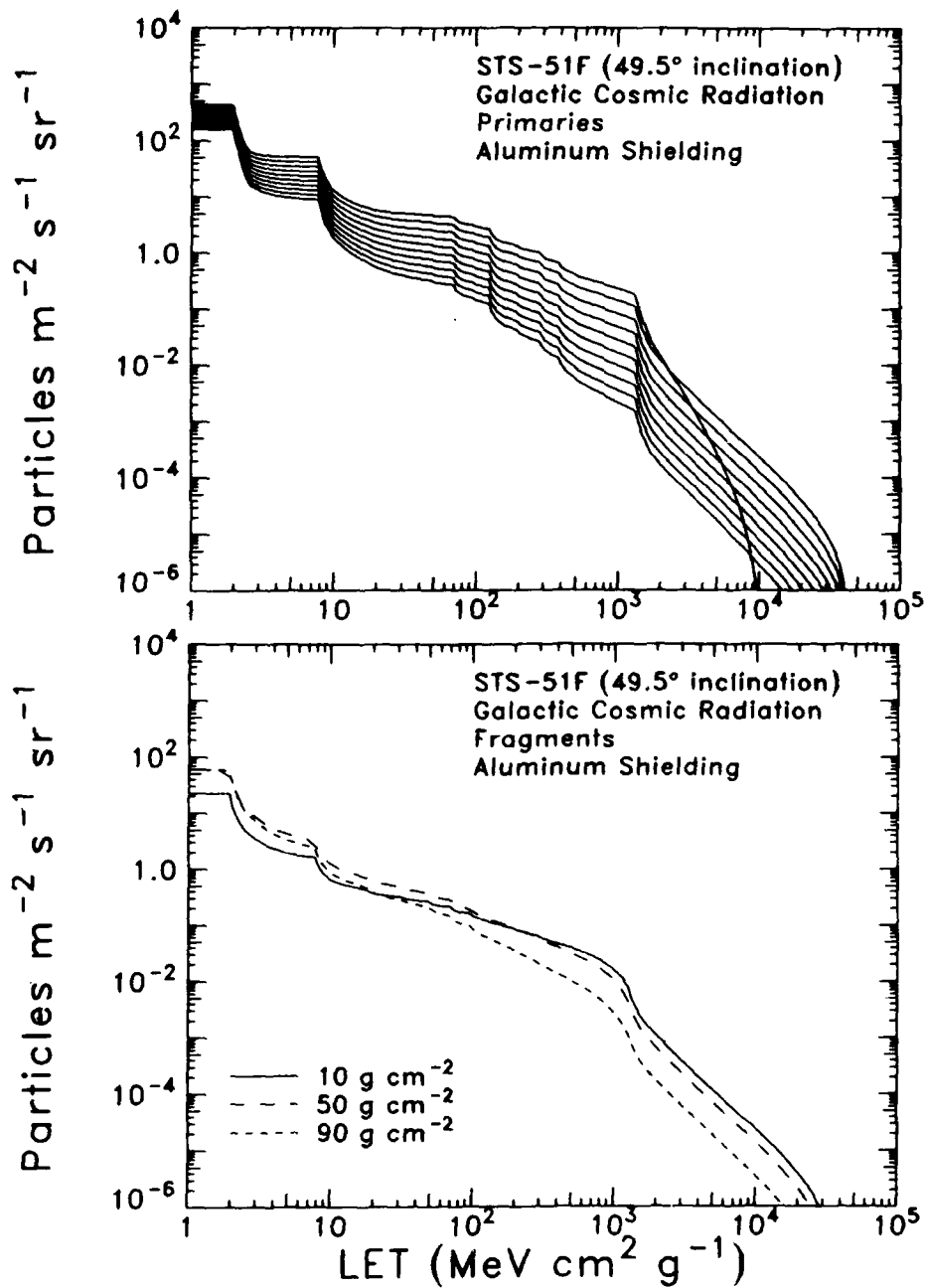


FIGURE 15
LET SPECTRA OF GALACTIC COSMIC RADIATION
POLAR ORBIT

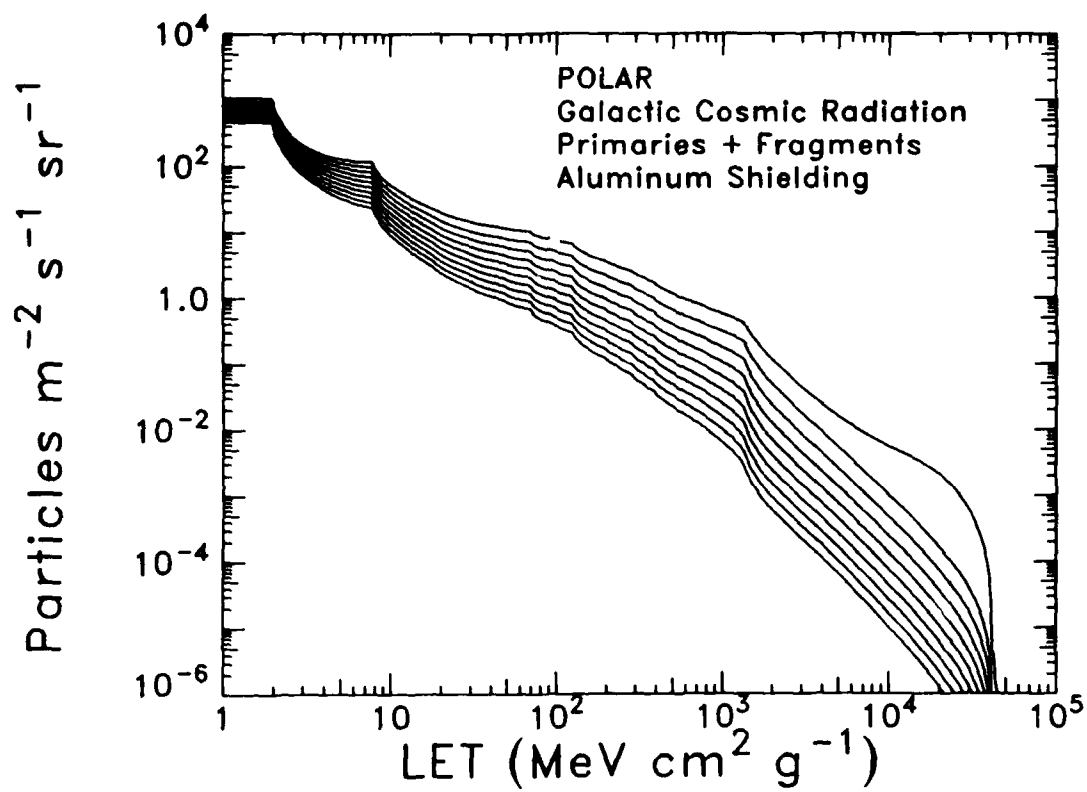


FIGURE 16
LET SPECTRA OF GALACTIC COSMIC RADIATION
DECOMPOSITION INTO PRIMARIES AND FRAGMENTS

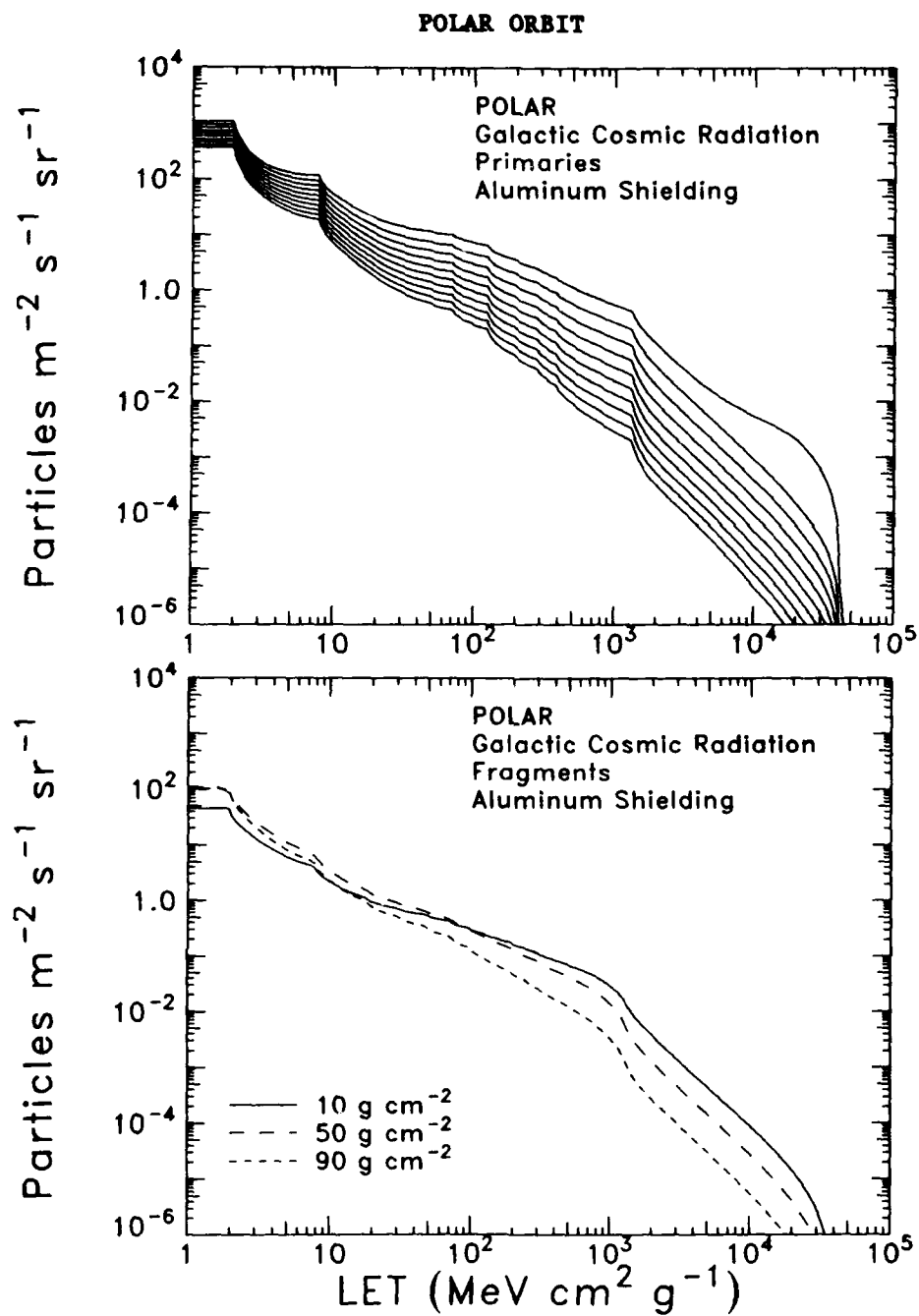


FIGURE 17
LET SPECTRA OF GALACTIC COSMIC RADIATION
EXO-MAGNETOSPHERE

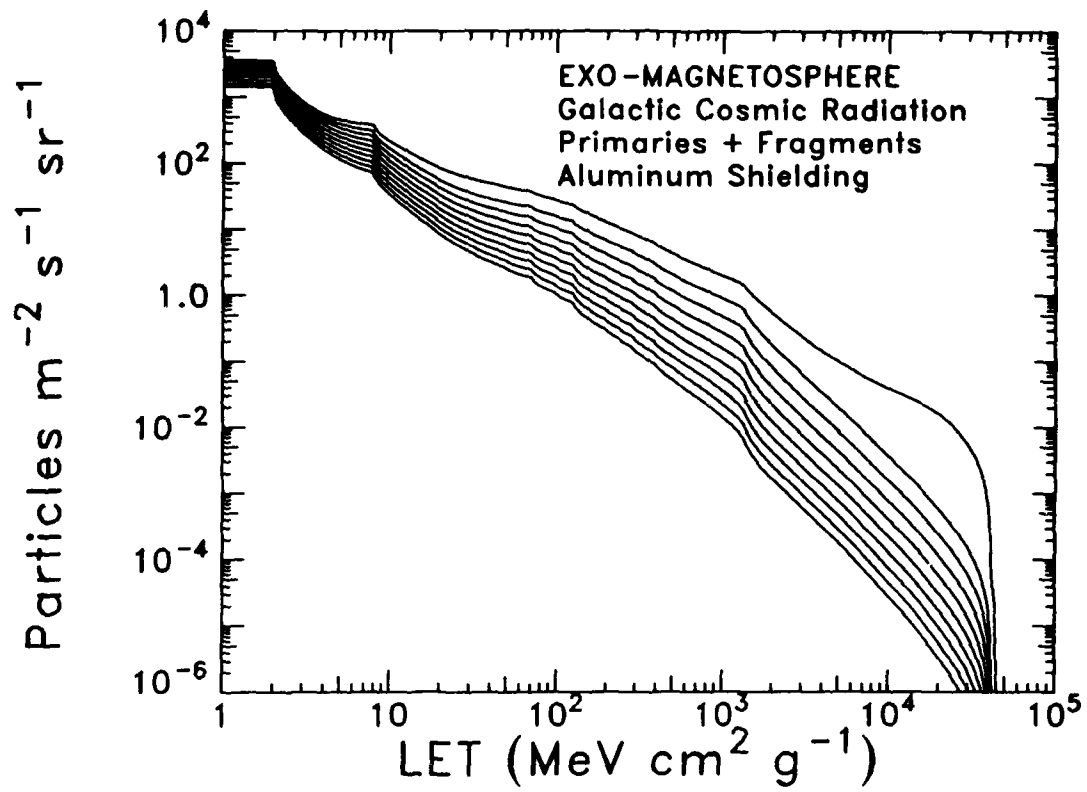
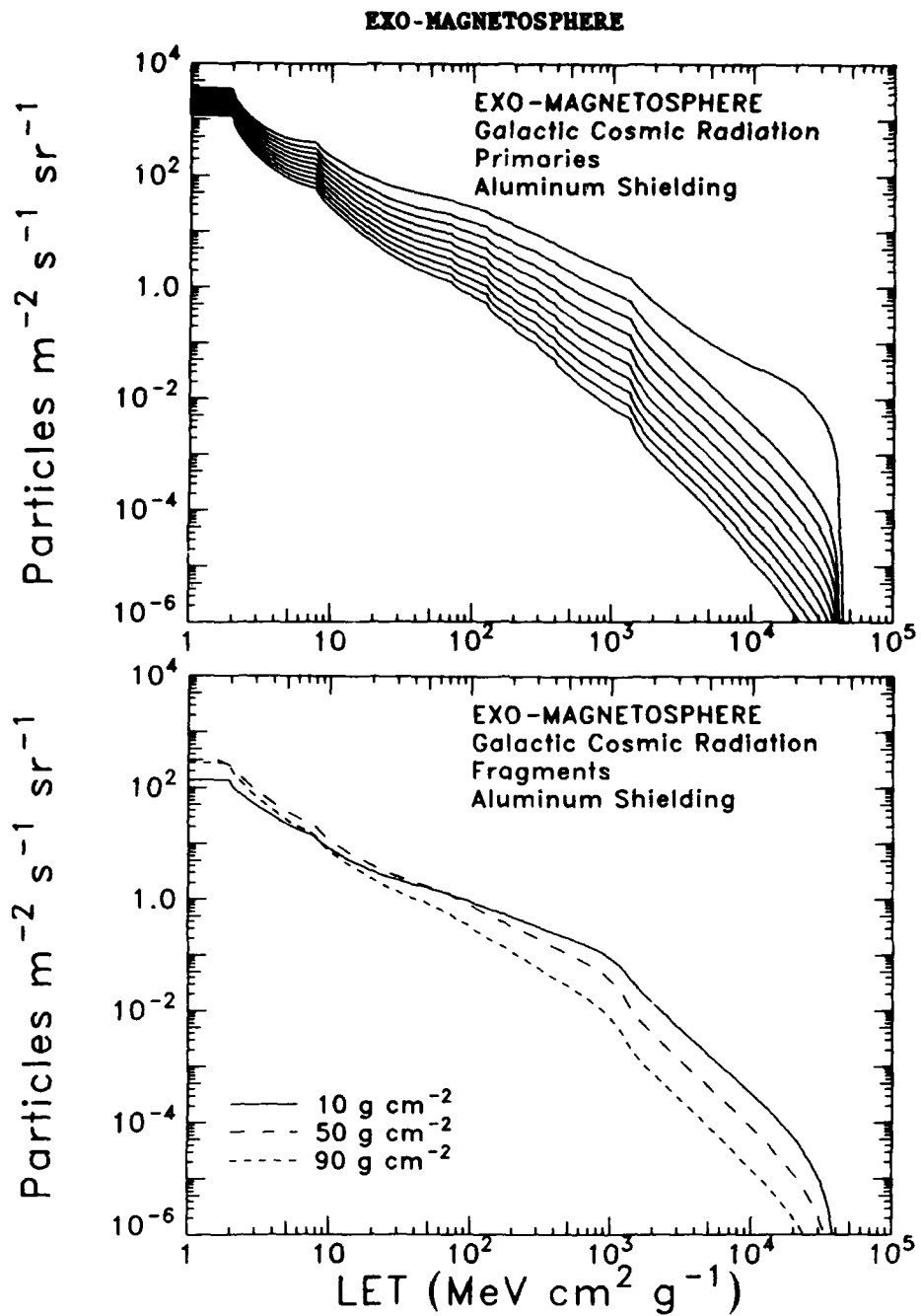


FIGURE 18

LET SPECTRA OF GALACTIC COSMIC RADIATION
 DECOMPOSITION INTO PRIMARIES AND FRAGMENTS



ABSORBED DOSE AND DOSE EQUIVALENT

Figures 19 through 23 show the annual absorbed dose and dose equivalent on the five spaceflights discussed in this paper. The results here represent only the contribution of galactic cosmic radiation and its fragments; trapped proton and target fragment contributions are not included.

The figures show a range of absorbed doses from approximately 0.1 cGy yr^{-1} to 15 cGy yr^{-1} depending on orbital configuration and shielding thickness. Likewise, the dose equivalents vary over the range 0.25 cSv yr^{-1} to 90 cSv yr^{-1} .

Both absorbed dose and dose equivalent are correlated with shielding thickness and orbital inclination. At higher inclinations there is less geomagnetic shielding and, consequently, more intense cosmic radiation. In no case is the fall in primary dose counteracted by fragment production. Fragments have lower charges and lower quality factors than their progenitors. Equilibrium fragment production is approached after 20 g cm^{-2} shielding.

The graphs of the dose and dose equivalent for polar orbit (Figure 22) and outside the magnetosphere (Figure 23) show anomalous behavior below 1 g cm^{-2} . As stated in an earlier section, the low-energy cosmic ray flux is not well known. The rough approximation of the CREME model, i.e., constant below 10 MeV per nucleon, leads to a dose equivalent outside the magnetosphere which is approximately 10 cSv yr^{-1} higher than extrapolations from larger shielding thicknesses would lead one to expect. The "skin dose" with no shielding shown in Figures 22 and 23 may be somewhat lower or substantially higher than indicated.

On each of the five missions, dose equivalent decreases more rapidly with increasing shielding than absorbed dose. This characteristic is expected because protons make a larger relative contribution to absorbed dose than to dose equivalent. Protons are absorbed by shielding more slowly than heavy ions. None of the curves shown exhibit simple exponential decline.

Differing functional dependencies of the absorbed dose and dose equivalent indicate that the quality of the radiation is dependent on shielding. Table 2 shows mean quality factors for each of the five missions at several shielding thickness. As expected, the mean quality factor decreases as heavy ions are fragmented and absorbed. The effect is slightly more pronounced for high inclination orbits where heavy ion fluxes have lower mean energy. The mean quality factor is both shielding dependent and significantly greater than 1. This demonstrates that the absorbed dose (cGy or rad) is not a useful measure of the biological effectiveness of galactic cosmic radiation. The dose equivalent gives a reasonable characterization of the radiation quality which is accurate to the extent that the quality factor reflects actual RBES.

TABLE 2

MEAN QUALITY FACTORS

<u>Flight</u>	<u>No Shielding</u>	<u>20 g cm⁻²</u>	<u>90 g cm⁻²</u>
STS-61C	4.9	3.6	1.8
STS-51J	4.9	3.6	1.8
STS-51F	5.1	3.5	1.6
POLAR	5.3	3.0	1.4
EXO-MAGNETOSPHERE	5.3	2.7	1.3

Figures 24 through 28 show the contributions of each element from hydrogen through nickel ($1 \leq Z \leq 28$) to the dose equivalent for 1 g cm^{-2} and 20 g cm^{-2} aluminum shielding. Within this shielding range, iron (Fe) is the single most important elemental component of the dose equivalent. It is slightly exceeded by protons only in the thick shielding case for the exo-magnetospheric mission. Iron makes up a greater percentage of the dose equivalent for low-inclination orbits than for high-inclination orbits. Elements in the charge range $15 \leq Z \leq 25$ are fragmentation products of iron and increase in importance with shielding.

Other elements of importance are identified in the figures. It is of interest to note that while the GCR abundances of carbon and oxygen are nearly the same, $\text{Dose}_O > \text{Dose}_C$ in all cases. Likewise, the GCR abundances of neon, magnesium, and silicon are nearly the same, yet $\text{Dose}_{Si} > \text{Dose}_{Mg} > \text{Dose}_N$ in all cases. The dose equivalent contribution of helium is about half the contribution of hydrogen (protons), though the He/H ratio is ~ 0.1 in GCR.

The relative importance of higher-charged cosmic ray species indicated above results from their increased energy deposition rate and their higher quality factors. This concept is of great importance in risk estimation. A cosmic-ray iron nucleus ($Z=26$) deposits energy at a rate $Z^2 = 676$ times greater than a cosmic-ray proton ($Z=1$). The absorbed dose in tissue (cGy or rad) from the iron nucleus is therefore 676 times greater than the dose from the proton. In addition to the energy deposition rate, the quality factor of iron is about 20 relative to protons. The dose equivalent in tissue (cSv or rem) from the iron nucleus is therefore ~ 13000 times greater than from the proton.

Figure 29 shows the percent contribution of fragments to the dose equivalent for each of the five missions at 20 g cm^{-2} and 90 g cm^{-2} . Fragments make no contribution to the radiation dose at zero shielding thickness. The absolute contribution of fragments is maximized at about 20 g cm^{-2} . The relative contribution of fragments continues to increase to the largest shielding thicknesses considered in this report.

Fragments contribute about 15% of the dose equivalent at 20 g cm^{-2} and between 30% and 40% of the dose equivalent at 90 g cm^{-2} . It is therefore clear that fragments of galactic-cosmic-ray heavy ions are a *significant component* of the dose equivalent to astronauts; however, they are *never the dominant component*.

The fragment contributions illustrated in Figure 29 provide an important consideration for the definition of astronaut radiation dosimetry research programs. Nuclear spallation cross sections, particularly partial cross sections for the spallation of nuclei on nuclei, are an imposing data gap in the present transport calculations. These cross sections are functions of many parameters, including energy, target charge and mass, projectile charge and mass, and product charge and mass. Only a minute fraction of these cross sections has been measured. For the practical purpose of computing galactic cosmic radiation doses to astronauts, a rough approximation of the partial cross sections is sufficient because fragments make up only a fraction of the GCR radiation dose.

FIGURE 19

ANNUALIZED ABSORBED DOSE AND DOSE EQUIVALENT

STS-61C

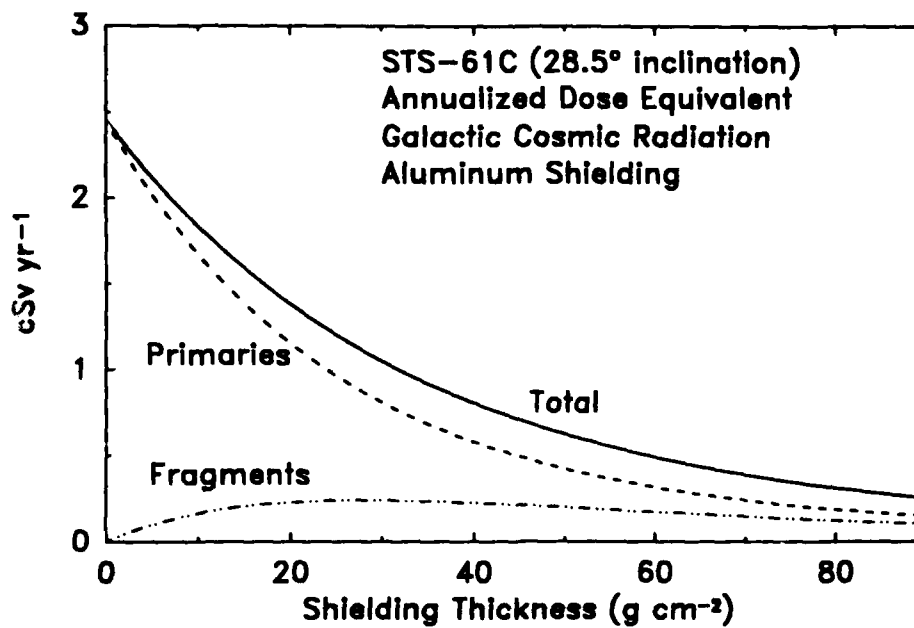
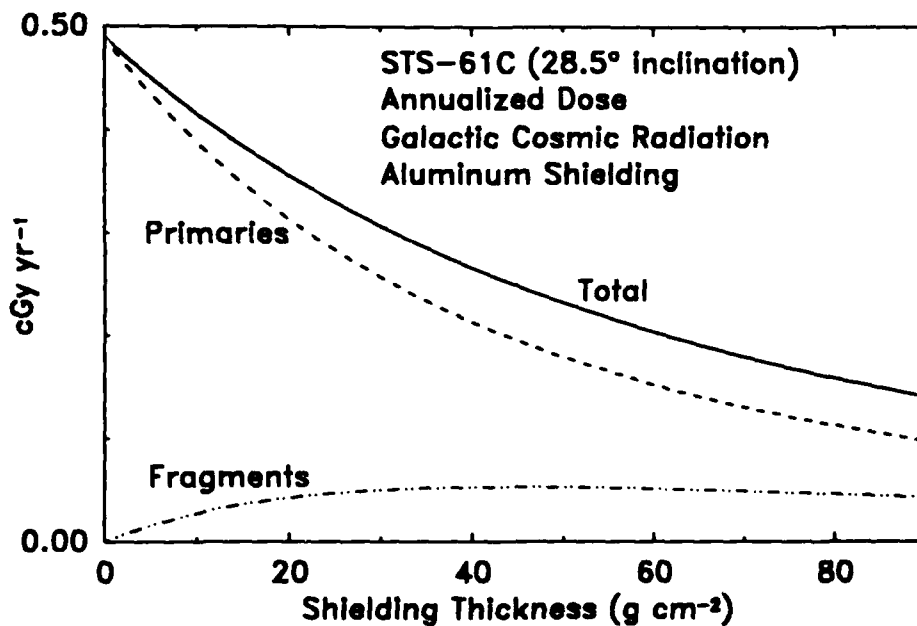


FIGURE 20
ANNUALIZED ABSORBED DOSE AND DOSE EQUIVALENT
STS-51J

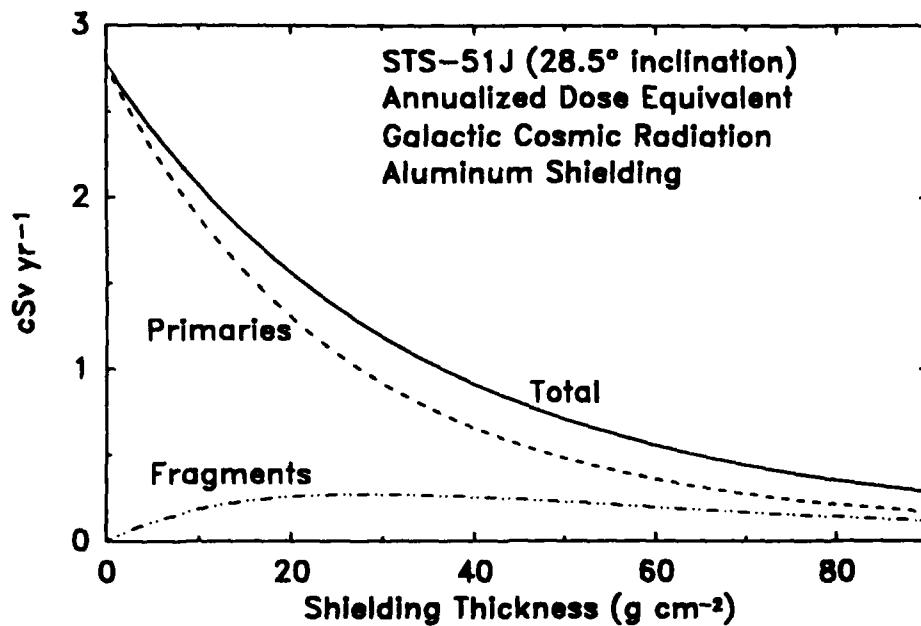
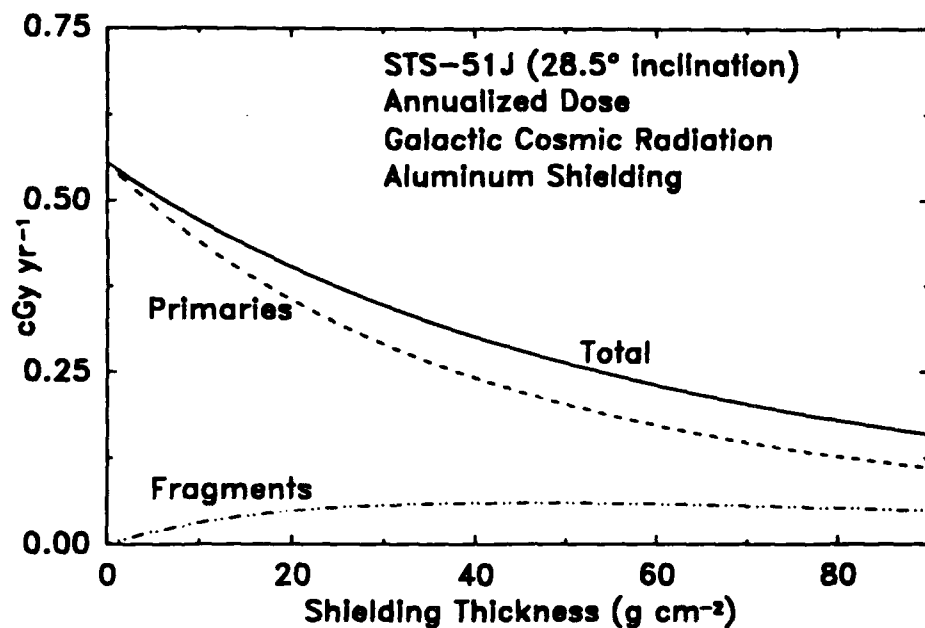


FIGURE 21

ANNUALIZED ABSORBED DOSE AND DOSE EQUIVALENT

STS-51F

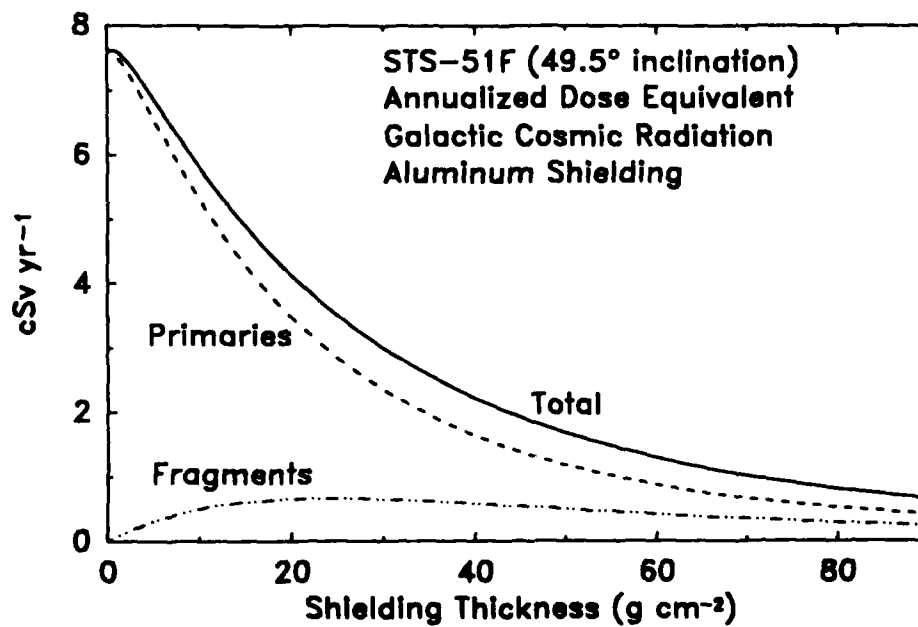
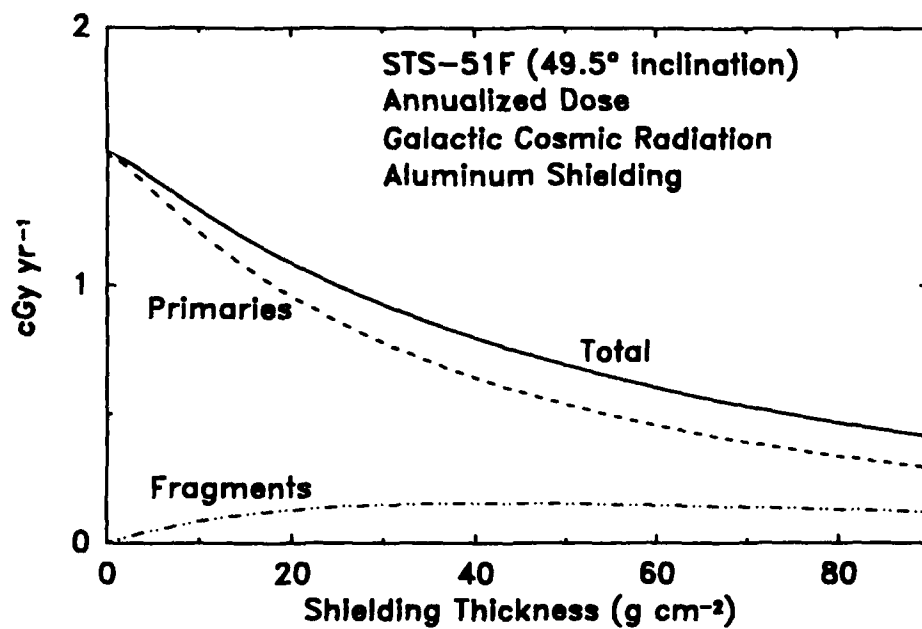


FIGURE 22
ANNUAL ABSORBED DOSE AND DOSE EQUIVALENT
POLAR ORBIT

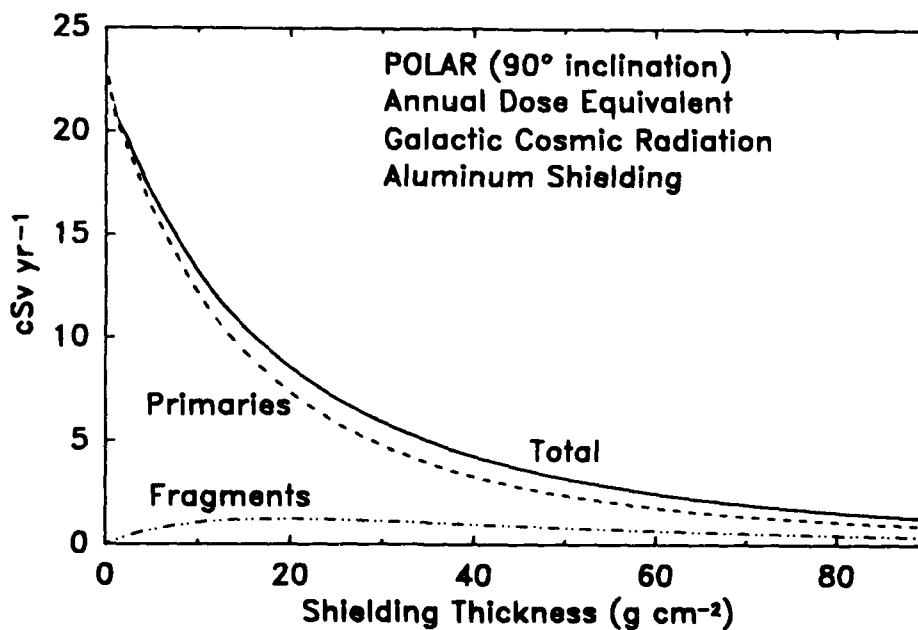
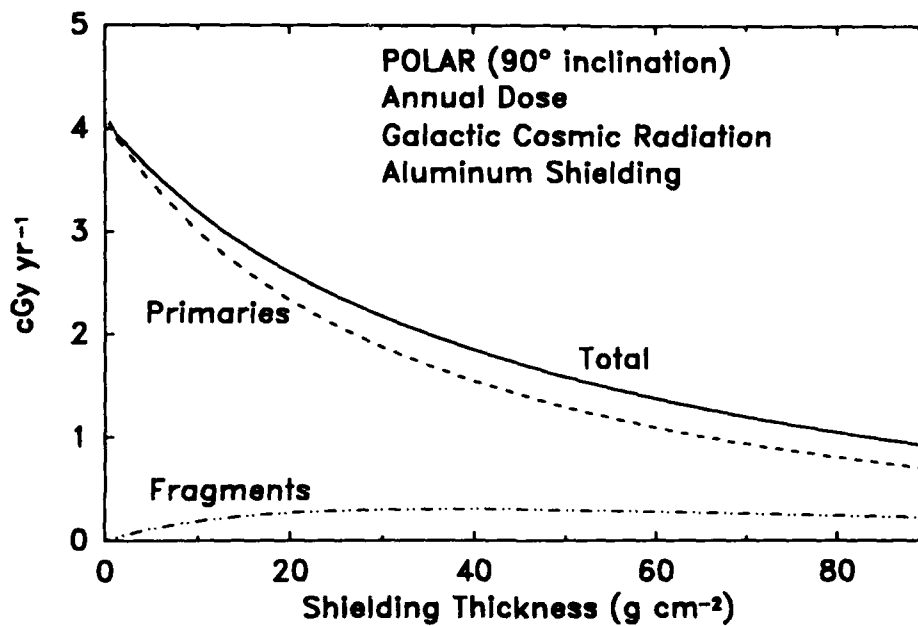


FIGURE 23

ANNUAL ABSORBED DOSE AND DOSE EQUIVALENT

EXO-MAGNETOSPHERE

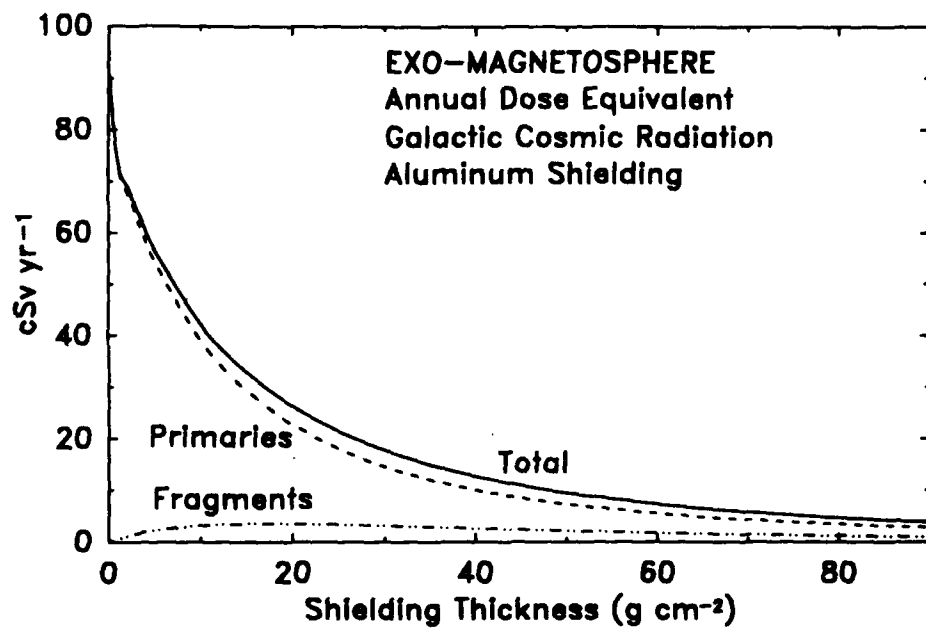
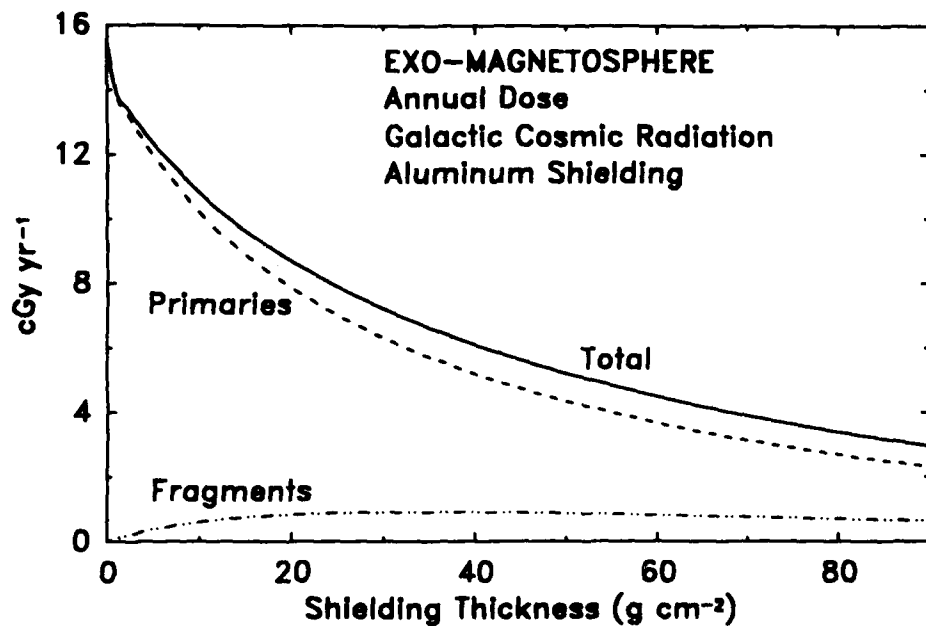


FIGURE 24

ELEMENTAL CONTRIBUTIONS TO ABSORBED DOSE AND DOSE EQUIVALENT

STS-61C

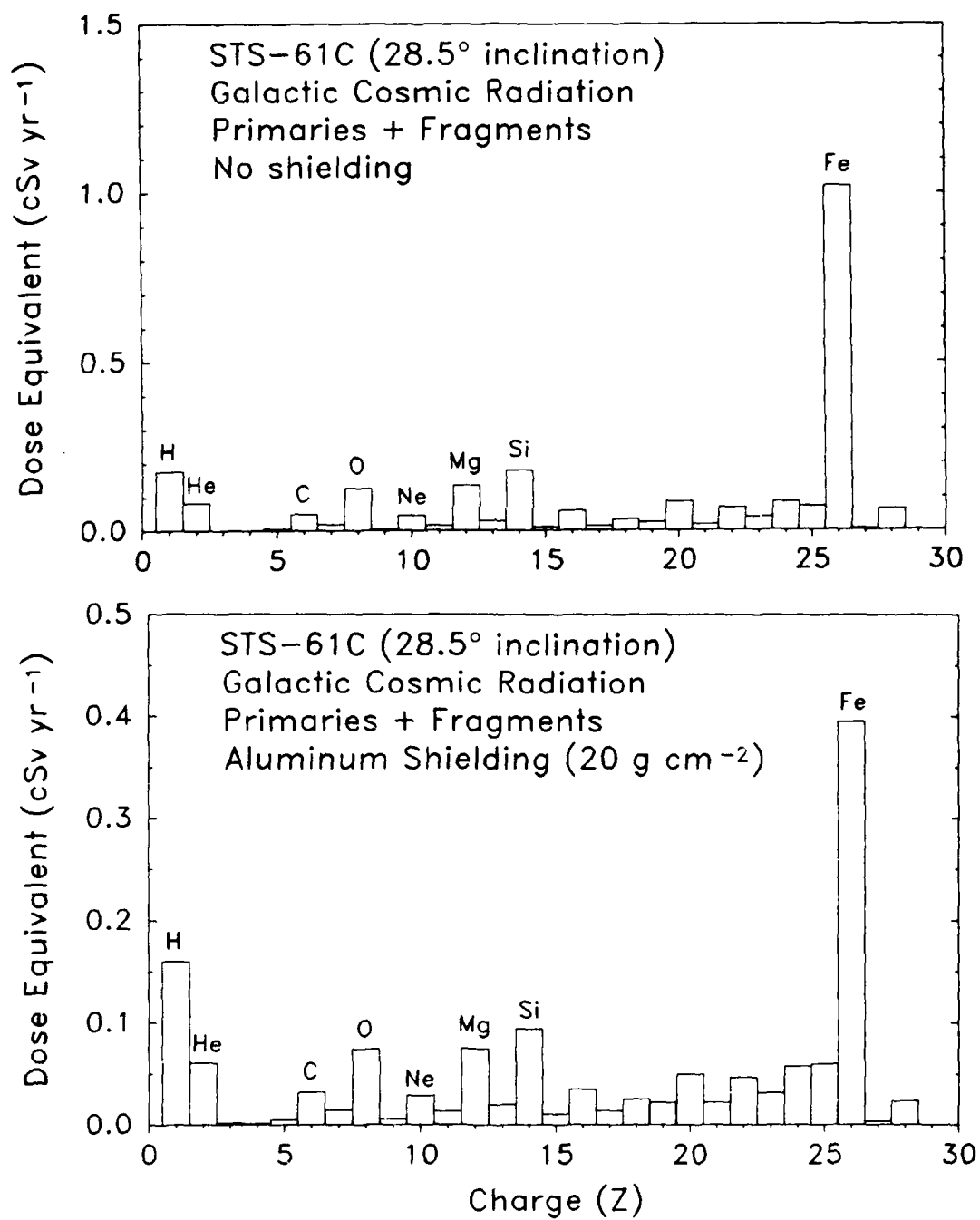


FIGURE 25

ELEMENTAL CONTRIBUTIONS TO ABSORBED DOSE AND DOSE EQUIVALENT

STS-51J

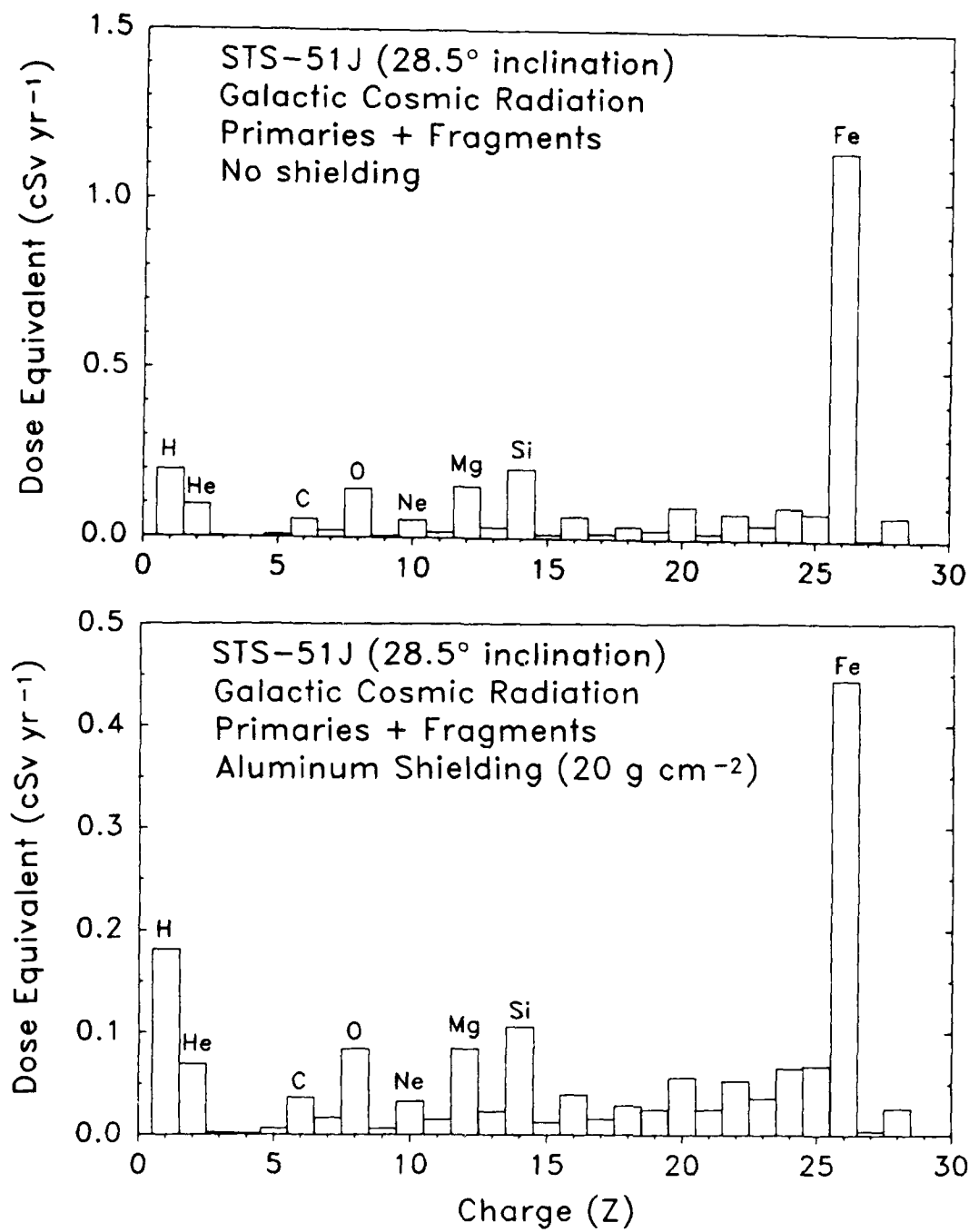


FIGURE 26

ELEMENTAL CONTRIBUTIONS TO ABSORBED DOSE AND DOSE EQUIVALENT

STS-51F

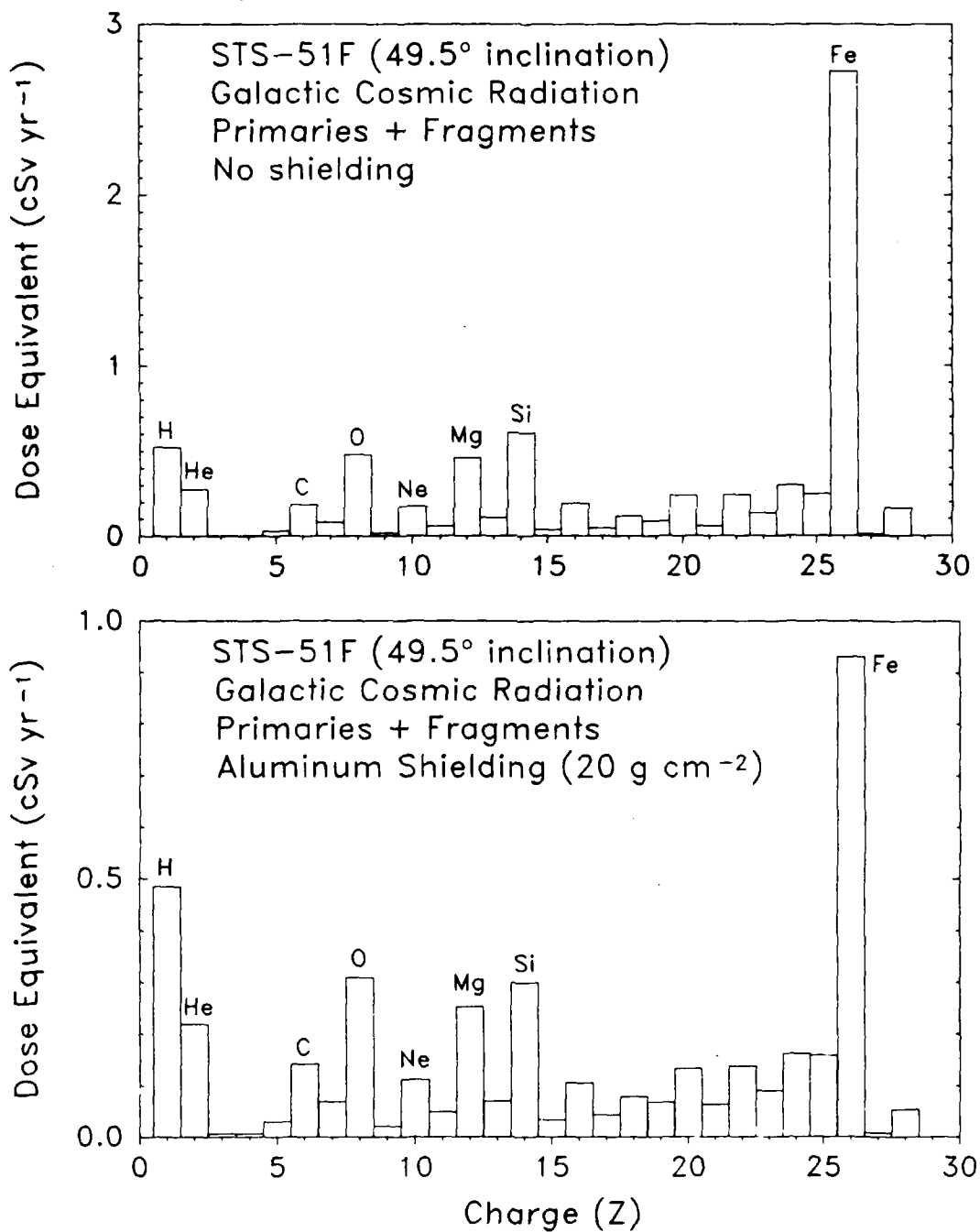


FIGURE 27

ELEMENTAL CONTRIBUTIONS TO ABSORBED DOSE AND DOSE EQUIVALENT

POLAR ORBIT

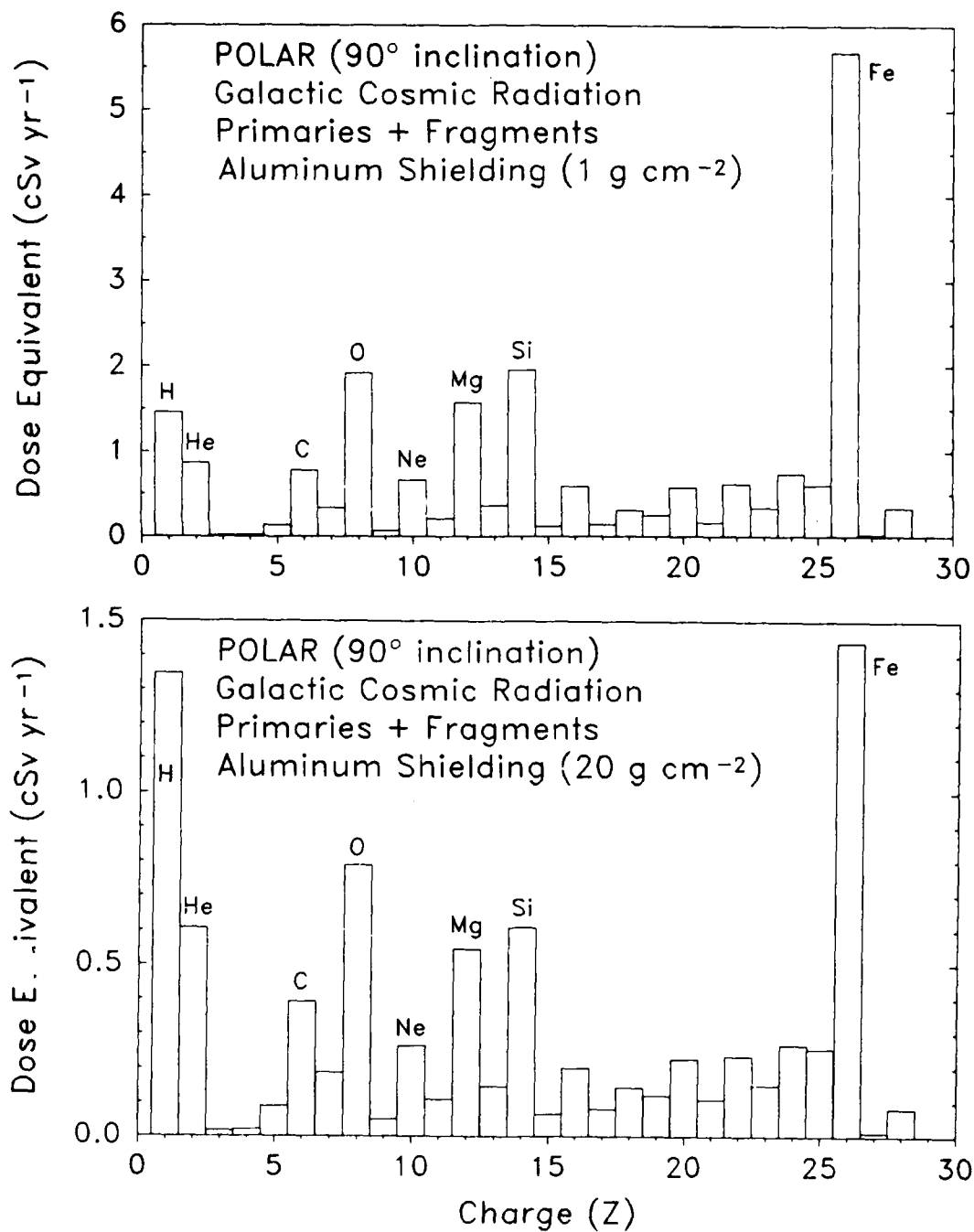


FIGURE 28

ELEMENTAL CONTRIBUTIONS TO ABSORBED DOSE AND DOSE EQUIVALENT

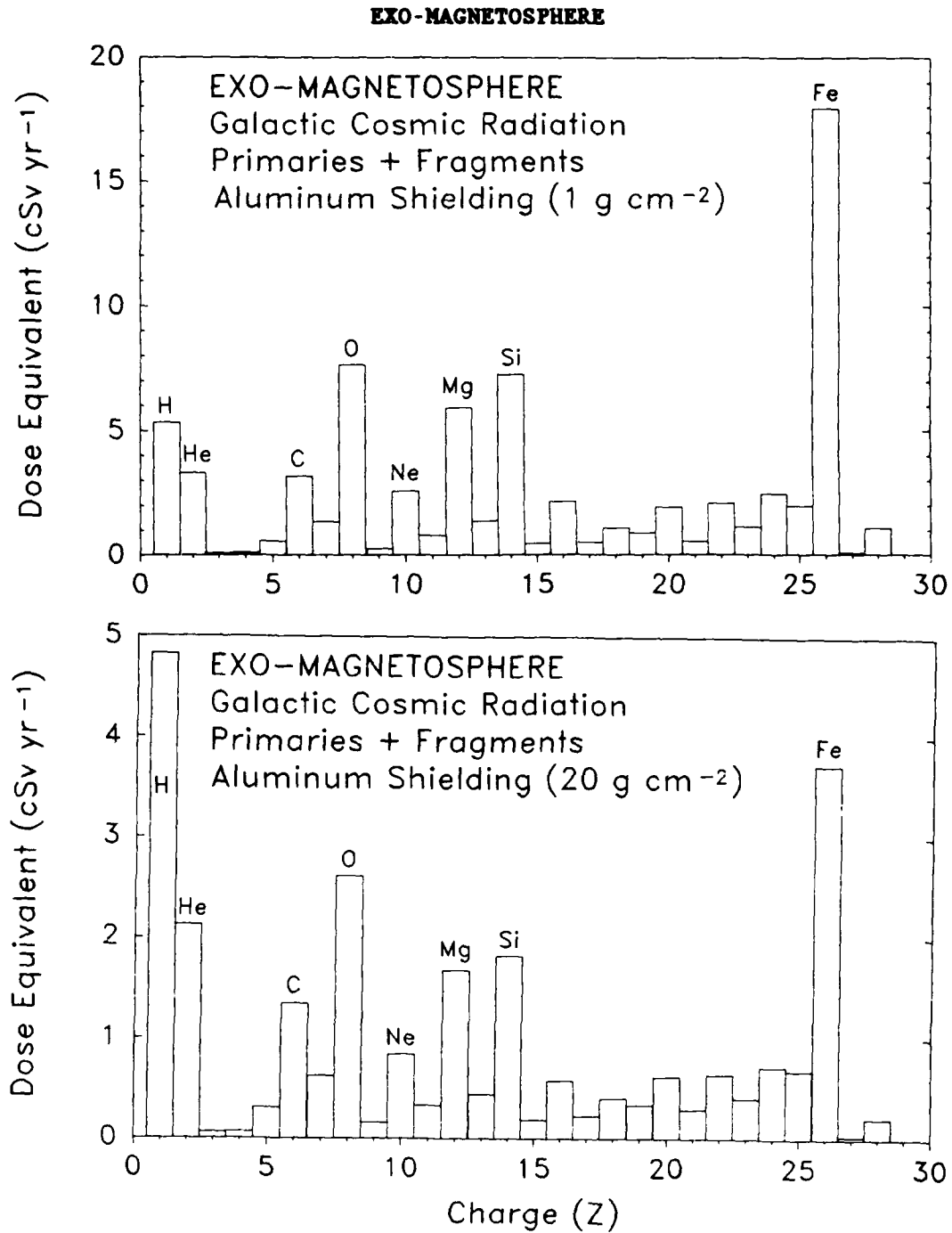
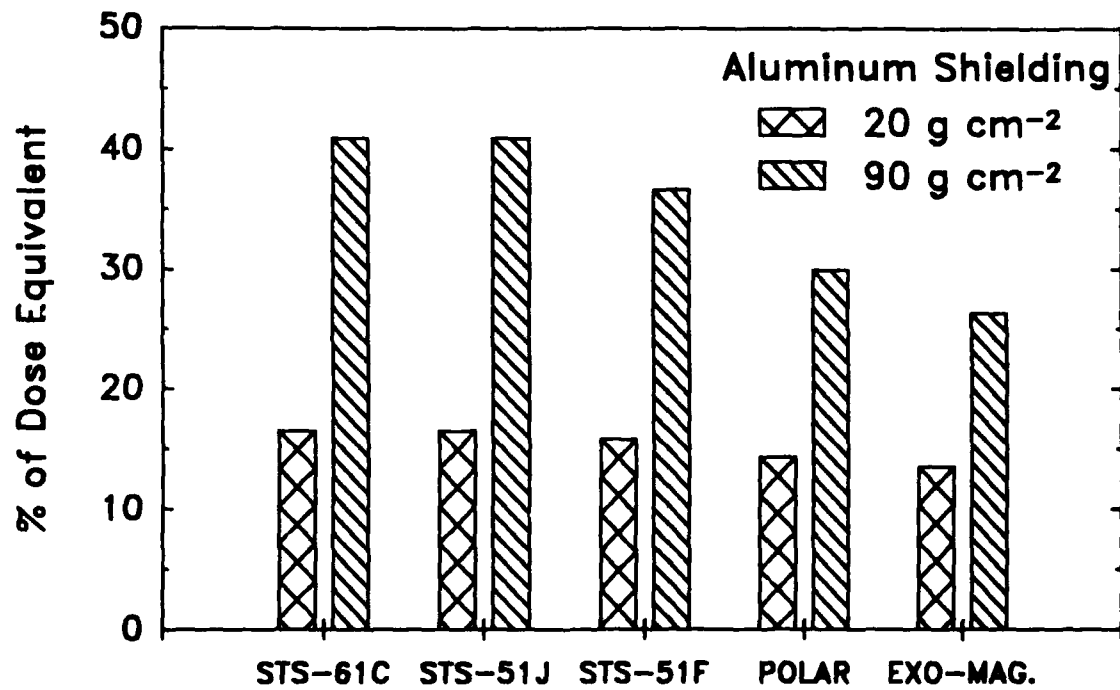


FIGURE 29
GALACTIC COSMIC RADIATION
FRACTIONAL CONTRIBUTION OF FRAGMENTS TO DOSE EQUIVALENT



SUMMARY AND CONCLUSIONS

LET spectra, absorbed dose, and dose equivalent from galactic cosmic radiation have been computed as a function of aluminum shielding thickness in the range 0 g cm^{-2} to 90 g cm^{-2} for five missions. The missions include low and high-altitude, low-inclination orbits; a high inclination orbit; polar orbit; and a mission outside the magnetosphere. The quantities calculated vary by two orders of magnitude over the range of parameters considered.

With 10 g cm^{-2} shielding the annual dose equivalents are: 1.8 cSv (low-altitude, low-inclination), 2.1 cSv (high-altitude, low-inclination), 5.8 cSv (high-inclination), 13.2 cSv (polar), and 42.4 cSv (exo-magnetosphere). These are "skin doses" behind aluminum shielding; they roughly approximate bone marrow doses behind 4 g cm^{-2} aluminum shielding. The contribution of target secondaries is not included in these estimates.

The dose equivalent is dominated by iron for thin shielding ($< 20 \text{ g cm}^{-2}$) and by protons for thicker shielding. Many other cosmic-ray species contribute significantly to the dose equivalent. The nuclear interaction cross sections and stopping powers of high-energy ions in aluminum are proportional to charge; hence, the mean quality factor decreases by about a factor of 4 over the shielding thicknesses considered. It is not possible to adequately characterize this variation in radiation quality using a pure energy-deposition unit such as absorbed dose.

The contribution of nuclear fragments to the GCR dose is significant, but never dominant. For practical applications, exact knowledge of the partial fragmentation cross sections is unnecessary because moderate errors cannot greatly affect the total dose.

REFERENCES

- Adams, J.H., Letaw, J.R. and Smart, D.F. 1983, "Cosmic Ray Effects on Microelectronics, Part II: The Geomagnetic Cutoff Effects," NRL Memorandum Report 5402, Naval Research Laboratory, Washington, D.C.
- Adams, J.H., Silberberg, R. and Tsao, C.H. 1981, "Cosmic Ray Effects on Microelectronics, Part I: The Near-Earth Particle Environment," NRL Memorandum Report 4506, Naval Research Laboratory, Washington, D.C.
- Ahlen, S.P. 1980, Theoretical and Experimental Aspects of the Energy Loss of Relativistic Heavy Ionizing Particles, Rev. Mod. Phys. 52, 121.
- Fry, R.J.M. 1986, Adv. Sp. Res. 6, 261-268.
- Heinrich, W. 1988, Variation of Galactic Cosmic Radiation by Solar Modulation, Geomagnetic Shielding and Shielding by Material, in "Terrestrial Space Radiation and Its Biological Effects," P.D. McCormack, C.E. Swenberg, and H. Bückner (eds.), Plenum, New York (in press).
- ICRP 1977, "Recommendations of the ICRP," Publication 26, Ann. ICRP 1, Pergamon, Oxford.
- ICRU 1986, "The Quality Factor in Radiation Protection," Report of a Joint Task Group of the ICRP and the ICRU to the ICRP and the ICRU, ICRU Report 40, International Commission on Radiation Units and Measurements, Bethesda, Maryland.
- Letaw, J.R. 1983, Proton Production Cross Sections in Proton-Nucleus Collisions, Phys. Rev. G28, 2178.
- Letaw, J.R. and Adams, J.H. 1986a, Comparison of CREME Model LET Spectra with Spaceflight Dosimetry Data, SCC Report 86-01, Severn Communications Corporation, Severna Park, Maryland.
- Letaw, J.R. and Adams, J.H. 1986b, Comparison of CREME Model LET Spectra with Spaceflight Dosimetry Data, IEEE Trans. Nucl. Sci. NS-33, 1620.
- Letaw, J.R. and Clearwater, S.H. 1986, "Radiation Shielding Requirements on Long-Duration Space Missions," SCC Report 86-02, Severn Communications Corporation, Severna Park, Maryland.
- Letaw, J.R., Silberberg, R. and Tsao, C.H. 1983, Proton-Nucleus Total Inelastic Cross Sections: An Empirical Formula for $E > 10$ MeV, Ap. J. Suppl. 51, 271.
- Letaw, J.R., Silberberg, R., Tsao, C.H. and Adams, J.H. 1985, Geometric Considerations in Single Event Upset Estimation, IEEE Trans. Nucl. Sci. NS-32, 4212-4215.

Letaw, J.R., Silberberg, R. and Tsao, C.H. 1986, Natural Radiation Hazards on the Manned Mars Mission, in "Manned Mars Mission (Working Group Papers)," NASA MO02, II, p. 642, NASA, Washington, D.C.

Letaw, J.R., Silberberg, R. and Tsao, C.H. 1987, Radiation Hazards on Space Missions, Nature 330, 709-710.

Letaw, J.R., Silberberg, R. and Tsao, C.H. 1988, Galactic Cosmic Radiation Doses to Astronauts Outside the Magnetosphere, in "Terrestrial Space Radiation and Its Biological Effects," P.D. McCormack, C.E. Swenberg, and H. Bückner (eds.), Plenum, New York (in press).

McCormack, P.D., Swenberg, C.E. and Bückner, H. (eds.) 1988, "Terrestrial Space Radiation and its Biological Effects," Plenum, New York (in press).

Northcliffe, L.C. and Schilling, R.F. 1970, Range and Stopping-Power Tables for Heavy Ions, Atomic Nucl. Data Tables A7, 233-463.

Olson, D.L., Berman, B.L., Greiner, D.E., Heckman, H.H., Lindstrom, P.J., and Crawford, H.J. 1983, Factorization of fragment-production cross sections in relativistic heavy-ion collisions, Phys. Rev. C28, 1602-1612.

Silberberg, R. and Tsao, C.H. 1973, Partial Cross Sections in High Energy Nuclear Reactions and Astrophysical Applications, Ap. J. Suppl. 25, 315.

Silberberg, R. and Tsao, C.H. 1977, Calculations of nucleus-nucleus cross sections and attenuation of complex cosmic ray nuclei in the atmosphere, Proc. 15th Int. Cosmic Ray Conf. 2, 89-94.

Silberberg, R., Tsao, C.H., Adams, J.H. and Letaw, J.R. 1984, Radiation Doses and LET Distributions of Cosmic Rays, Rad. Res. 98, 209.

Silberberg, R., Tsao, C.H. and Letaw, J.R. 1985, Improved Cross Sections for Astrophysical Applications, Ap. J. Suppl. 58, 873.

Westfall, G.D., Wilson, L.W., Lindstrom, P.J., Crawford, H.J., Greiner, D.E. and Heckman, H.H. 1979, Fragmentation of Relativistic ^{56}Fe , Phys. Rev. C19, 1309-1323.

Ziegler, J.F. 1980, "Handbook of Stopping Cross Sections for Energetics Ions in All Elements," v. 5, Pergamon, New York.